69 P

NASA CR-145365

Simplified Multiple Scattering Model for Radiative Transfer in Turbid Water

A.H. Ghovanlou

J.N. Gupta

Metrek Division of The MITRE Corporation

1820 Dolley Madison Blvd.

McLean, Virginia 22101

Contract No. F19628-77-C-0001

May 1978

National Aeronautics and Space Administration

Langley Research Center

Hampton, Virginia 23665

ERRATA

NASA Contractor Report 145365

SIMPLIFIED MULTIPLE SCATTERING MODEL FOR RADIATIVE TRANSFER IN TURBID WATER

A. H. Ghovanlou
J. N. Gupta

Metrek Division of the MITRE Corporation
May 1978

Page 2-6: The final sentence should read "The Fresnel transmission coefficient which takes into account the refraction due to the transmission from water into the air has been left out of Equation (11)."

Page 2-7, equation (13): The integration limits should be from - 1 to 0 rather than from - 1 to + 1.

Page 2-17, equation (35b); page 2-18, equation (36); the equation on page 4-1; page 4-10, equation (42):

The denominator of the integrand in these equations should be

$$\mu^2 \sin^2 W + \cos^2 W$$

It should be noted that these errors were typographical and that results presented in the paper are correct as printed.

NASA CR-145365

Simplified Multiple Scattering Model for Radiative Transfer in Turbid Water

A.H. Ghovanlou
J.N. Gupta

Metrek Division of The MITRE Corporation
1820 Dolley Madison Blvd.
McLean, Virginia 22101

Contract No. F19628-77-C-0001
May 1978

National Aeronautics and
Space Administration

Langley Research Center
Hampton, Virginia 23665

ABSTRACT

Quantitative analytical procedures for relating selected water quality parameters to the characteristics of the backscattered signals, measured by remote sensors, require the solution of the radiative transport equation in turbid media. In this paper, we present an approximate closed form solution of this equation and based on this solution discuss the remote sensing of the sediments. The results are compared with other standard closed form solutions such as quasi-single scattering approximations.

ACKNOWLEDGMENT

The authors would like to thank Dr. R. G. Henderson for his valuable advice on the content and organization of this report.

The authors would also like to express their appreciation to Olga Jackson for her excellent support and patience in preparing the manuscript of this report.

TABLE OF CONTENTS

LIST OF ILLUSTRATIONS

LIST OF TABLES

1.0 INTRODUCTION

The emergence of new environmental regulations restricting coastal zone developments combined with the desirability of developing coastal areas for energy and other important activities, and finally expansion of coastal jurisdiction to a two hundred mile zone, make fast response monitoring capabilities, possible by remote sensing applications, an attractive option. The question may be raised, why remote sensing is not employed on a larger than presently utilized scale. The answer lies simply in the inadequacy of quantitative procedures for obtaining water quality information from remotely sensed data. Presently several governmental, and industrial programs are addressing these inadequacies. Among these is a laboratory program at NASA-Langley Research Center (LaRC). The basic experimental setup and the goals of this program are described below.

The purpose of the LaRC laboratory program is to determine whether the spectral characteristic of the upwelling radiance can be related to the amount and properties of the particulates and other pollutants. In the LaRC experimental setup, the beam of a solar simulator illuminates a large water tank filled with turbid water; the water turbidity in the tank is generated by the stepwise introduction of known amounts of sediments and other materials of known properties. An overhead detector system including a spectrometer, electronics, and a camera, measures the strengths and the characteristics

of the upwelling radiance signal in the wavelengths range of 300-1100 nm.

The Metrek Division of the Mitre Corporation has been assisting LaRC in the area of radiative transfer modeling. In the past, Metrek's modeling approach has been based on Monte Carlo simulation techniques [1,2]. These techniques were originally selected to avoid mathematical complexities involved in the analytical solution to the radiative transport equation resulting from the inclusion of the geometry of the tank, in which the LaRC's laboratory experiment is conducted. Recent application of Metrek's Monte Carlo simulation model has shown that the inclusion of the tank geometry may not be necessary for high turbidity levels (attenuation coefficient $\alpha \geq 4$ meter^{-1}) of interest to the LaRC program. Other factors which may lead to the same conclusion with regard to the tank geometry considerations are:

- Small reflectivity of the tank boundaries ($\approx$ 3.0 percent)
- Large dimensions of the tank (diameter = 2.6 meter, height = 3 meter)
- Small footprint of the overhead detector (circular spot of radius = 3.5 cm).

The smallness of the footprint of the detector permits another simplifying situation. With this, it may be assumed that the incident radiation (spot size 30 cm) behaves like a plane wave as far as the radiation emerging through the footprint of the detector is concerned.

The simplified geometry, and the plane wave assumption, described above, allow the derivation of an approximate solution to the radiative transfer equation in turbid water.

The present report discusses this closed form solution and illustrates the variations in the upwelling radiance for situations which are of interest in remote sensing applications. In order to establish common notation the optical parameters of the turbid water are described in the next section.

1.1 Optical Parameters of Turbid Water

In the absence of polarization the following parameters are necessary for optical characterization of turbid water:

- Total absorption coefficient, a.
- Total scattering coefficient, s.

These coefficients have the dimension of meter^{-1}. The attenuation coefficient, α, is the sum of the absorption and scattering coefficients. The single scattering albedo, $\tilde{\omega}_o$, is defined as the ratio of total scattering to the total attenuation coefficient.

Another parameter of interest is the scattering phase function $P(\theta)$. This function specifies the angular pattern of the scattering of a collimated beam from an infinitesimal volume of turbid water. The scattering probability function $P_F(\mu)$, for polar angle ($\theta = \cos^{-1} \mu$) is defined in terms of the scattering phase function by:

$$P_F(\mu) = \frac{\int_{\mu}^{1} P(\mu)\, d\mu}{\int_{-1}^{1} P(\mu)\, d\mu}$$

for all μ between -1 and +1.

1.2 Summary

The purpose of this work is to provide a closed form analytical expression which will enable the Langley Researchers to verify their experimental results, and/or to optimize their experimental parameters without considerable theoretical calculations.

In Section 2, the mathematical formalism applicable to the radiative transport process is established for the geometry of the light scattering relevant to the LaRC laboratory set up experiment. The analytical solution to the equation of radiative transfer is then derived for the backscattered radiance, as a function, of $\tilde{\omega}_0$, incident radiance I_0, and an appropriate representation of the scattering phase function $P(\mu)$ in the form $P(\mu) = F\,\delta(\mu-1) + B$.* This representation adequately displays the properties of the scattering phase functions for turbid water (i.e., a strong peak in the forward direction), and at the same time allows derivation of a closed form solution to the radiative transfer equation.

In Section 3 the results on measured as well as calculated scattering phase functions have been summarized. The measured phase

*F, and B are constants, and δ is the Dirac Delta function.

functions represent a wide range of turbid water conditions. The calculated scattering phase functions are arrived at utilizing the Mie formalism for polydispersed suspensions and the size distribution measurements provided through the LaRC Laboratory program. Acceptable values for B, are then obtained using measured as well as calculated phase functions results. It is found that B varies between 0.007 (for a Feldspar particulate distribution calculated from the Mie formalism) and 0.0585 (for measured San Diego Harbor Water). F can be shown to be related to B by F = 2-2B (see Section 2.2).

Section 4 presents the numerical results determined from the solution of the radiative transfer equation obtained in Section 2.0. The backscattered radiance is calculated for various values of $\tilde{\omega}_o$ and B. $\tilde{\omega}_o$ is the single scattering albedo and varies with wavelength, λ.* Typical values of the a/s ratio at 550 nm may vary between 0.06 (for quartz particles) and 0.20 for natural waters [3]. The a/s ratio for sediments as a function of wavelength may vary between 0.20 at λ = 550 nm and 0.50 at λ = 370 nm [4]. The results generated in this work are compared with those of Gordon [5], who used a quasi-single scattering approximation solution. For smaller values of $B(\approx 0.02)$, and $\tilde{\omega}_o(\approx 0.80)$ the difference in the two results is of the order of 15 percent. At higher values of $\tilde{\omega}_o(\approx 0.95)$ and $B(\approx 0.06)$, the difference in the two results is significant.

*Specifically $\tilde{\omega}_o = \frac{s(\lambda)}{s(\lambda) + a(\lambda)} = (1 + \frac{a(\lambda)}{s(\lambda)})^{-1}$, where λ is the wavelength.

2.0 SOLUTION TO THE RADIATIVE TRANSFER EQUATION

2.1 Radiative Transfer Equation For An Idealized Geometry Case

The radiative transfer equation in any medium may be written as (6)

$$\hat{\eta} \cdot \nabla I(\vec{r},\hat{\eta}) + \alpha(\vec{r})\, I(\vec{r},\hat{\eta}) = \frac{S(\vec{r})}{4\Pi} \int d\Omega(\hat{\eta}') \, P(\hat{\eta},\hat{\eta}') \, I(\vec{r},\hat{\eta}') \qquad (1)$$

where $I(\vec{r},\hat{\eta})$, (see Figure 2.1) represents the radiance of a given frequency, at the position defined by $\vec{r}$ and in the direction designated by the unit vector $\hat{\eta}$. $P(\hat{\eta},\hat{\eta}')$ is the scattering phase function, and $\hat{\eta}$ is the scattering angle. $P(\hat{\eta},\hat{\eta}')$ does not include any polarization effects and satisfies the condition:

$$\frac{1}{4\Pi} \int P(\hat{\eta},\hat{\eta}') \, d\Omega(\hat{\eta}') = 1 \quad . \qquad (1a)$$

$d\Omega(\hat{\eta}')$ denotes the differential solid angle about $\hat{\eta}'$. A rigorous derivation of Equation (1) together with a discussion of its range of validity may be found in the literature [7,8].

Equation (1) may be specialized for an ideal case of an incident plane wave in which the incident light is unpolarized and is normally falling on a homogeneous half space. The homogeneous half space is represented by an attenuation coefficient, α, and a scattering coefficient, s. Under these conditions Equation (1) becomes:

$$\mu \frac{\partial I(z,\mu)}{\partial z} + \alpha \, I(z,\mu) = \frac{s}{2} \int P(\mu,\mu') \, I(z,\mu') \, d\mu' \qquad (2)$$

FIGURE 2.1
A GEOMETRY OF THE LIGHT SCATTERING PROBLEM

μ is the cosine of angle θ shown in Figure 2-1. Extensions to the geometries other than the one considered here are straight forward and will not be discussed in this report.

Using the transformation $\alpha z=\tau$, and defining $\tilde{\omega}_o = \frac{s}{\alpha}$, we obtain

$$(\mu \frac{\partial}{\partial \tau} + 1)\ I(\tau,\mu) \ = \ \frac{\tilde{\omega}_o}{2} \int \ P(\mu,\mu')\ I(\tau,\mu')\ d\mu' \ . \qquad (3)$$

2.2 The Scattering Phase Function $P(\mu,\mu')$

The phase function $P(\mu,\mu')$ for a variety of turbid waters have been studied in a previous report [1]. In general, these functions show a very strong peak in the forward direction. As a result of this the standard method of solution to the equation of radiative transfer, which is based on the expansion of $P(\mu,\mu')$ in terms of Legendre polynomials is not practical. Legendre polynomial expanstions involve large number of terms and result in a large number of coupled differential equations.

A representation which displays the properties of the phase functions for turbid water and at the same time enables us to seek an analytical solution to the radiative transport equation is given by the distribution:

$$P(\mu,\mu') \ = \ F\ \delta(\mu-\mu') + B \qquad (4)$$

where δ is the Dirac delta function, $B << F$, and

$$F + 2B = 2 \qquad (4a)$$

Equation (4a) is the result of substituting Equation (4) in Equation (1a).

2.3 Treatment of Multiple Scattering

Upon substitution of Equation (4) in Equation (3) it may be shown that

$$\mu \frac{\partial I}{\partial \tau} + I(\tau,\mu) \left[1 - \frac{\tilde{\omega}_o F}{2}\right] = \frac{\tilde{\omega}_o B}{2} \int I(\tau,\mu') \, d\mu' \tag{5a}$$

On taking the Laplace transform of both sides, we obtain

$$\mu \left[s \, \phi(s,\mu) - I(o,\mu)\right] + \left(1 - \frac{\tilde{\omega}_o F}{2}\right) \phi(s,\mu) = \frac{\tilde{\omega}_o B}{2} \phi_o(s) \tag{5b}$$

here $$\phi(s,\mu) = \int_o^\infty I(\tau,\mu) \, e^{-\tau s} \, d\tau \quad , \text{ and}$$

$$\phi_o(s) = \int_{-1}^{1} \phi(s,\mu) \, d\mu$$

Rearranging terms in Equation (5b) results in

$$\phi(s,\mu) = \frac{\frac{\tilde{\omega}_o B}{2} \phi_o(s) + \mu I(o,\mu)}{1 + \mu s - \tilde{\omega}_o F/2} \tag{6a}$$

Integrating both sides w.r.t. μ we get

$$\phi_o(s) = \frac{\int_{-1}^{1} \left[\mu\, I\left(o,\mu\right) \Big/ \left(1 - \frac{\tilde{\omega}_o F}{2} + \mu s\right) \right] d\mu}{1 - \frac{B\tilde{\omega}_o}{2s} \ln \left[\left(1 - \frac{\tilde{\omega}_o F}{2} + s\right) \Big/ \left(1 - \frac{\tilde{\omega}_o F}{2} - s\right) \right]} \tag{6b}$$

Equation (6b) can be further simplified if it is considered that

$$I(o,\mu) = I_o\, \delta(\mu-1) \qquad \text{for } \mu > o$$

$$= I(o,\mu) \qquad \text{to be determined for } \mu < o$$

This means that the radiance just below the water surface and traveling in the water is the same as the incident radiance. $I(o,\mu)$ for $\mu < o$ is determined from the relationship between ϕ_o and $I(o,\mu)$ obtained from Equation (6a) by substituting $s = -\left(1 - \frac{\tilde{\omega}_o F}{2}\right) \Big/ \mu$, and may be written as

$$I(o,\mu) = -\frac{\tilde{\omega}_o B}{2\mu}\ \phi_o \left[-\left(1 - \frac{\tilde{\omega}_o F}{2}\right) \Big/ \mu \right] \tag{7}$$

Equation (6b) then reduces to:

$$\phi_o(s) = \frac{\dfrac{I_o}{1 - \frac{\tilde{\omega}_o F}{2} + s} - \dfrac{\tilde{\omega}_o B}{2} \displaystyle\int_{-1}^{o} \frac{\phi_o\left[-\left(1 - \frac{\tilde{\omega}_o F}{2}\right) \Big/ \mu \right]}{1 - \frac{\tilde{\omega}_o F}{2} + \mu s}\, d\mu}{1 - \frac{B\tilde{\omega}_o}{2s} \ln \left[\left(1 - \frac{\tilde{\omega}_o F}{2} + s\right) \Big/ \left(1 - \frac{\tilde{\omega}_o F}{2} - s\right) \right]} \tag{8}$$

2.4 Quasi-Single Scattering Approximation

Before we discuss a more complete solution to Equation (8) we show how quasi-single scattering approximation can be derived from the present formulation, and study the assumptions underlying this approximation.

The quasi-single scattering approximation as developed by Gordon [5] corresponds to neglecting terms which include B in Equation (8), i.e.,

$$\phi_o(s) = I_o \Big/ \left(1 - \frac{\tilde{\omega}_o F}{2} + s\right) \tag{9}$$

which upon making use of Equation (7) results in:

$$I(o,\mu) = \frac{B\tilde{\omega}_o}{2\left(1 - \tilde{\omega}_o F/2\right)} \cdot \frac{I_o}{\left(1 + |\mu|\right)} \tag{10}$$

A further assumption in the derivation of the quasi-single scattering approximation is the substitution of B in Equation (10) by $P(-|\mu|)$. Considering this the resultant quasi-single scattering approximation becomes

$$I(o,\mu) = \frac{\tilde{\omega}_o P(-|\mu|)}{2\left(1 - \tilde{\omega}_o F/2\right)} \cdot \frac{I_o}{\left(1 + |\mu|\right)} \tag{11}$$

The Fresnel transmission coefficient which takes into account the reflraction due to the transmission from water into the air has been left out of Equation (11).

2.5 Derivation of a Simplified Multiple Scattering Solution

Here the Equation in point is (8). The denominator of Equation (8) displays complex singularity characteristics (because of the branches of the log-function) in the physical range of the variables of interest. The derivation of the solution of interest is thus based on an analytical continuation technique. In what follows we discuss the characteristics of the various terms in Equation (8), which may be re-written as:

$$\left(1 - \frac{\tilde{\omega}_o F}{2} + s\right) \phi_o(s) = \frac{G(s)}{1 - \frac{B\tilde{\omega}_o}{2s} \ln\left[\left(1 - \frac{\tilde{\omega}_o F}{2} + s\right) \Big/ \left(1 - \frac{\tilde{\omega}_o F}{2} - s\right)\right]} \quad (12)$$

where

$$G(s) = I_o - \frac{\tilde{\omega}_o B}{2}\left(1 - \frac{\tilde{\omega}_o F}{2} + s\right) \int_{-1}^{1} \frac{\phi_o\left(-\frac{1 - \tilde{\omega}_o F/2}{\mu}\right)}{1 - \frac{\tilde{\omega}_o F}{2} + \mu s} d\mu \quad (13)$$

The observations which can be made at this point are:

(1) $G(s)$ is regular for $\mathrm{Re}(s) < \left(1 - \frac{\tilde{\omega}_o F}{2}\right)$,

(2) $\phi_o(s)$ is regular for $\mathrm{Re}(s) > o$ (by definition),

(3) $\left(1 - \frac{\tilde{\omega}_o F}{2} + s\right)$ has a zero at $s = -\left(1 - \frac{\tilde{\omega}_o F}{2}\right)$,

(4) $-\frac{1}{2s}\ln\left[\left(1-\frac{\tilde{\omega}_o F}{2}+s\right)\Big/\left(1-\frac{\tilde{\omega}_o F}{2}-s\right)\right]$ is regular in the strip

$$-\left(1-\frac{\tilde{\omega}_o F}{2}\right) < \mathrm{Re}(s) < \left(1-\frac{\tilde{\omega}_o F}{2}\right)$$

The question to be answered now, concerns the zeros of the denominator of Equation (12). Two cases are to be distinguished (a) $3\left(\frac{1}{\tilde{\omega}_o}-1\right) < B$ which is satisfied only by a scattering medium with negligible absorption, and (b) $3\left(\frac{1}{\tilde{\omega}_o}-1\right) > B$. Only case (b) has physical significance for the case of radiative transfer in turbid water and is discussed in this report.

$$\text{Define } \tau(s) = 1 - \frac{B\tilde{\omega}_o}{2s}\ln\left[\left(1-\frac{\tilde{\omega}_o F}{2}+s\right)\Big/\left(1-\frac{\tilde{\omega}_o F}{2}-s\right)\right] \qquad (15a)$$

which may be re-written as

$$\tau(s) = \left[1 - \frac{1-\frac{\tilde{\omega}_o F}{2}}{2s}\ln\left\{\frac{1-\frac{\tilde{\omega}_o F}{2}+s}{1-\frac{\tilde{\omega}_o F}{2}-s}\right\}\right] + \frac{1-\tilde{\omega}_o}{2s}\ln\left\{\frac{1-\frac{\tilde{\omega}_o F}{2}+s}{1-\frac{\tilde{\omega}_o F}{2}-s}\right\} \qquad (15b)$$

For $s\to o$, the term in the capital brackets goes to zero like s^2, and the second term approaches the value $\left(\frac{1-\tilde{\omega}_o}{1-\tilde{\omega}_o F/2}\right)$. This implies that

$\tau(s)$ is analytic and non zero in the strip $-\left(1-\frac{\tilde{\omega}_o F}{2}\right) < \mathrm{Re}(s) < \left(1-\frac{\tilde{\omega}_o F}{2}\right)$. Furthermore, the function $\tau(s) \to 1$ as $|s| \to \infty$ in this strip.

The function $\tau(s)$ can be factored as [9]

$$\tau(s) = \frac{\tau_+(s)}{\tau_-(s)} \tag{16}$$

where $$\tau_{\mp}(s) = \mathrm{Exp}\left\{\frac{1}{2\pi i}\int_{\mp\beta-i\infty}^{\mp\beta+i\infty} \frac{\log \tau(z)}{z-s}\, dz\right\} \tag{17a}$$

with $\tau_+(s)$ regular for $\mathrm{Re}(s) < \beta$, and $\tau_-(s)$ regular for $\mathrm{Re}(s) < -\beta$ for some $o < \beta < \left(1-\frac{\tilde{\omega}_o F}{2}\right)$. Further, there exists a constant $C_1' > o$ and a number β' such that

$$\begin{aligned} |\tau_+(s)| &> C_1' \quad \text{for } \mathrm{Re}(s) < \beta' < \beta \\ |\tau_-(s)| &> C_1' \quad \text{for } \mathrm{Re}(s) > -\beta' > -\beta \end{aligned} \tag{17b}$$

Substitution of Equation (16) in Equation (12) results in

$$\left(1-\frac{\tilde{\omega}_o F}{2}+s\right)\frac{\phi_o(s)}{\tau_-(s)} = \frac{G(s)}{\tau_+(s)} \tag{18}$$

The function $\phi_o(s)$ is regular for $\mathrm{Re}(s) > o$, and $\tau_-(s)$ is regular and non zero for $\mathrm{Re}(s) > -\beta$. Thus the left hand side of Equation (18)

is regular for Re(s) > o. Furthermore, G(s) is regular for Re(s) < $\left(1 - \frac{\tilde{\omega}_o F}{2}\right)$, and $\tau_+(s)$ is regular and non zero for Re(s) < β. Hence the right side of Equation (18) is regular for Re(s) < β. Since β > o these two domains of regularity overlap, and in the strip o < Re(s) < β the right and left sides of Equation (18) are equal (see Figure 2.2). Therefore they are equal everywhere. From the principles of analytical continuation each side of Equation (18) is equal to a function H(s) which is regular in the entire complex s-plane. Since $G(s)/\tau_+(s)$ is bounded for $|s| \to \infty$, then from Liouville's theorem [10], the function H(s) = constant C_o and Equation (18) results in,

$$\phi_o(s) = C_o \frac{\tau_-(s)}{1 - \tilde{\omega}_o F/2 + s} \tag{19}$$

By letting $s \to o$ in Equations (19) and (6b) we have

$$C_o = \left(1 - \frac{\tilde{\omega}_o F}{2}\right) \left\{\lim_{s \to o} \phi_o(s)\right\} \Big/ \left\{\lim_{s \to o} \tau_-(s)\right\} \tag{20}$$

and $$\lim_{s \to o} \phi_o(s) = \left(\frac{I_o}{1 - \frac{\tilde{\omega}_o F}{2}}\right) \Big/ \left(\frac{1 - \tilde{\omega}_o}{1 - \frac{\tilde{\omega}_o F}{2}}\right)$$

$$= \frac{I_o}{1 - \tilde{\omega}_o} \tag{21}$$

Substitution of Equations (20) and (21) in Equation (19) results in

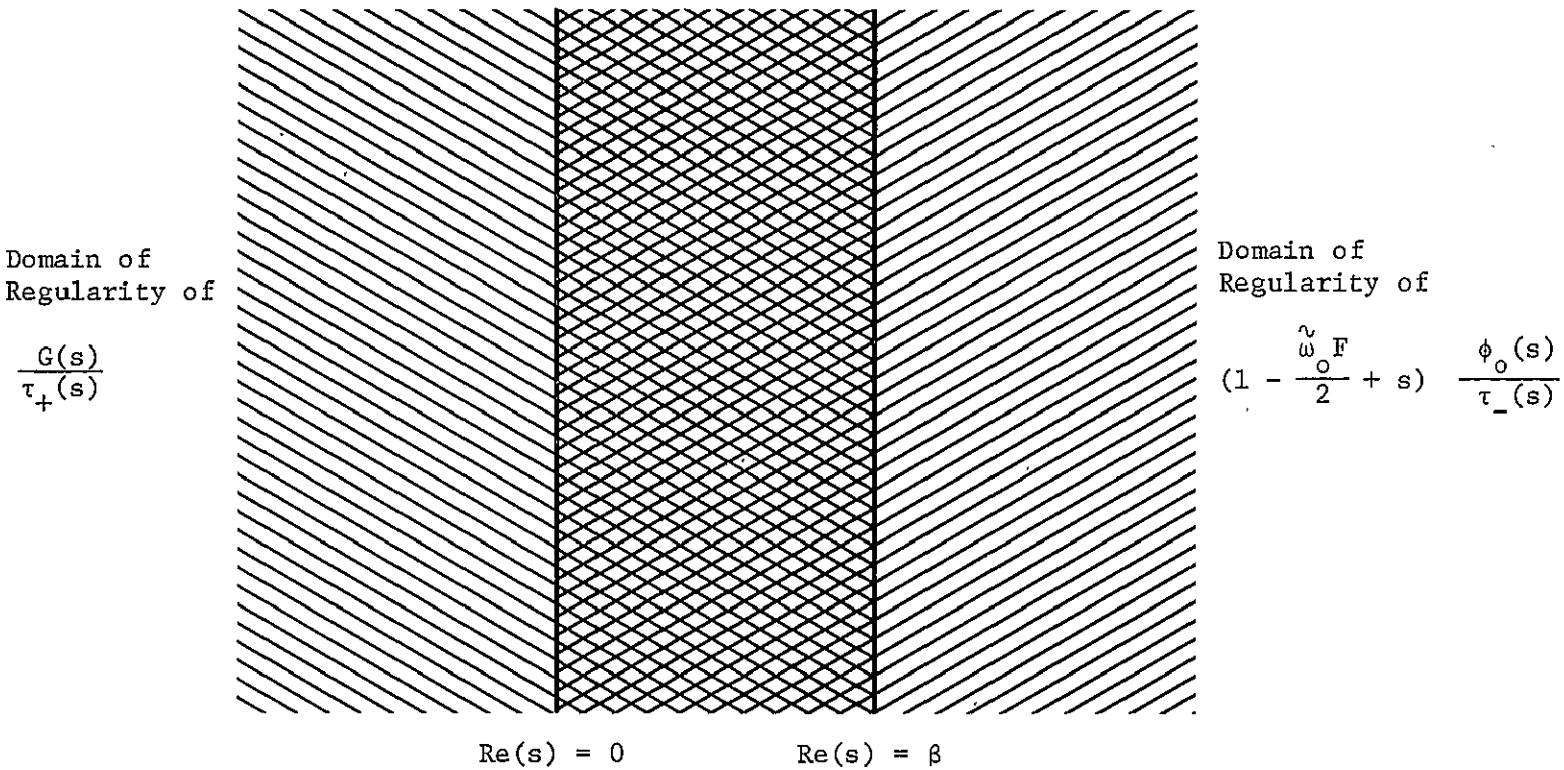

FIGURE 2.2
DOMAINS OF REGULARITY

$$\phi_o(s) = \frac{(1 - \tilde{\omega}_o F/2)\ I_o\ \tau_-(s)}{(1 - \tilde{\omega}_o)\ (1 - \tilde{\omega}_o F/2 + s)} \qquad \frac{1}{\lim_{s \to o} \left\{ \tau_-(s) \right\}} \tag{22}$$

From this equation, information about $I(o,\mu)$ may be obtained. In view of this we shall next determine $\tau_-(s)$ and $\lim_{s \to o} \tau_-(s)$.

The function $\tau_-(s)$ is written as (see Equation 17a):

$$\tau_-(s) = \text{Exp}\left\{ \frac{1}{2\pi i} \int_{-\beta-i\infty}^{-\beta+i\infty} \frac{\ln \tau(z)}{z-s}\ dz \right\}$$

or

$$\ln \tau_-(s) = \frac{1}{2\pi i} \int_{-\beta-i\infty}^{-\beta+i\infty} \frac{\ln \left[1 - \frac{B\tilde{\omega}_o}{2z}\ \ln \left(\frac{1 - \tilde{\omega}_o F/2 + z}{1 - \tilde{\omega}_o F/2 - z} \right) \right]}{z-s}\ dz \tag{23}$$

To put $\ln \tau_-(s)$, $\text{Re}(s) > o$ in a form more convenient than in Equation (23); we make use of the Canchy Goursat theorem (11). From the application of this theorem the path is shifted from the line $-\beta + iy$ $(-\infty < y < \infty)$ to the imaginary axis indented as shown in Figure 2.3. The contribution from the semicircle at $z=o$ goes to zero when $s \neq o$.

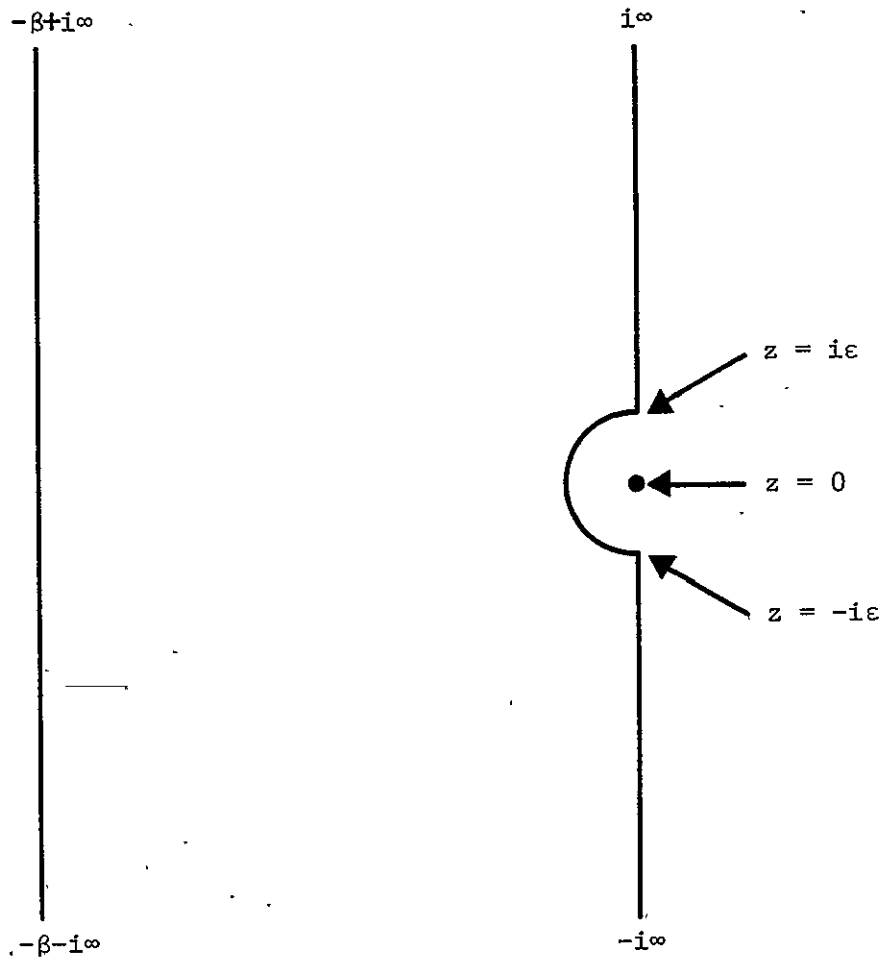

FIGURE 2.3
AN EXAMPLE OF A CONTOUR INTEGRAL

Since $s \neq o$ in Equation (23), therefore we obtain

$$\ln \tau_{-}(s) = \frac{1}{2\pi i} \int_{-i\infty}^{i\infty} \frac{\ln \left[1 - \frac{B\tilde{\omega}_o}{2z} \ln \left(\frac{1 - \tilde{\omega}_o F/2 + z}{1 - \tilde{\omega}_o F/2 - z} \right) \right]}{z - s} dz \quad (24)$$

Let $z = ix$

$$\text{then } \ln \tau_{-}(s) = \frac{1}{2\pi} \int_{-\infty}^{\infty} \frac{\ln \left[1 - \frac{B\tilde{\omega}_o}{x} \tan^{-1} \left(\frac{x}{1 - \tilde{\omega}_o F/2} \right) \right]}{ix - s} dx \quad (25)$$

Now substitute $\tan W = \frac{x}{1 - \tilde{\omega}_o F/2}$ for $x > o$, and $\tan W = -\frac{x}{1 - \tilde{\omega}_o F/2}$ for $x < o$. It will result in

$$\ln \tau_{-}(s) = \frac{1}{2\pi} \int_{o}^{\pi/2} \frac{\ln \left[1 - \frac{B\tilde{\omega}_o}{1 - \tilde{\omega}_o F/2} \cdot \frac{W}{\tan W} \right]}{i(1 - \tilde{\omega}_o F/2) \tan W - s} \left(1 - \frac{\tilde{\omega}_o F}{2} \right) \sec^2 W \, dW$$

$$+ \frac{1}{2\pi} \int_{o}^{\pi/2} \frac{\ln \left[1 - \frac{B\tilde{\omega}_o}{1 - \tilde{\omega}_o F/2} \cdot \frac{W}{\tan W} \right]}{-i(1 - \tilde{\omega}_o F/2) \tan W - s} \left(1 - \frac{\tilde{\omega}_o F}{2} \right) \sec^2 W \, dW$$

or

$$\ln \tau_{-}(s) = -\frac{s\left(1 - \frac{\tilde{\omega}_o F}{2}\right)}{\pi} \int_{o}^{\pi/2} \frac{\ln \left[1 - \frac{B\tilde{\omega}_o}{1 - \tilde{\omega}_o F/2} \cdot \frac{W}{\tan W} \right]}{(1 - \tilde{\omega}_o F/2)^2 \sin^2 W + s^2 \cos^2 W} dW \quad (26)$$

and

$$\tau_-(s) = \text{Exp}\left[-\frac{s\left(1-\frac{\tilde{\omega}_o F}{2}\right)}{\pi}\int_0^{\pi/2}\frac{\ln\left\{1-\frac{B\tilde{\omega}_o}{1-\tilde{\omega}_o F/2}\cdot\frac{W}{\tan W}\right\}}{\left(1-\frac{\tilde{\omega}_o F}{2}\right)^2\text{Sin}^2 W + s^2\,\text{Cos}^2 W}\,dW\right] \quad (27)$$

To evaluate $\lim_{s\to o}\tau_-(s)$, we first consider $\lim_{s\to o}\left[\tau_-(s)\right]$, which from Equation (24) is given by

$$\lim_{s\to o}\ln\tau_-(s) = \frac{1}{2\pi i}\int_{-i\infty}^{i\infty}\frac{\ln\left[1-\frac{B\tilde{\omega}_o}{2z}\ln\left(\frac{1-\tilde{\omega}_o F/2+z}{1-\tilde{\omega}_o F/2-z}\right)\right]}{z}\,dz \quad (28)$$

To take into account the contribution from the semicircle at z=o,

Equation (28) may be rewritten as

$$\lim_{s\to o}\left\{\ln\tau_-(s)\right\} = \lim_{\varepsilon\to o}\left[\frac{1}{2\pi i}\int_{-i\infty}^{-i\varepsilon}\frac{\ln\left\{1-\frac{B\tilde{\omega}_o}{2z}\ln\left(\frac{1-\frac{\tilde{\omega}_o F}{2}+z}{1-\frac{\tilde{\omega}_o F}{2}-z}\right)\right\}}{z}\,dz\right.$$

$$\left.+\frac{1}{2\pi i}\int_{-i\varepsilon}^{i\varepsilon}\frac{\ln\left\{1-\frac{B\tilde{\omega}_o}{2z}\ln\left(\frac{1-\frac{\tilde{\omega}_o F}{2}+z}{1-\frac{\tilde{\omega}_o F}{2}-z}\right)\right\}}{z}\,dz\right]$$

$$+\frac{1}{2\pi i}\int_{i\varepsilon}^{i\infty}\frac{\ln\left\{1-\frac{B\tilde{\omega}_o}{2z}\ \ln\left(\frac{1-\frac{\tilde{\omega}_o F}{2}+z}{1-\frac{\tilde{\omega}_o F}{2}-z}\right)\right\}}{z}dz \quad (29)$$

Let z=-ix in the first integral, and z=ix in the third integral of the right hand side of Equation (29). It will result in

$$\lim_{\varepsilon\to o}\ \frac{1}{2\pi i}\int_{-i\infty}^{-i\varepsilon}\frac{\ln\left\{1-\frac{B\tilde{\omega}_o}{2z}\ \ln\left(\frac{1-\tilde{\omega}_o F/2+z}{1-\tilde{\omega}_o F/2-z}\right)\right\}}{z}dz =$$

$$-\lim_{\varepsilon\to o}\ \frac{1}{2\pi i}\int_{i\varepsilon}^{i\infty}\frac{\ln\left\{1-\frac{B\tilde{\omega}_o}{2z}\ \ln\left(\frac{1-\tilde{\omega}_o F/2+z}{1-\tilde{\omega}_o F/2-z}\right)\right\}}{z}dz \quad (30)$$

Therefore,

$$\lim_{s\to o}\ \left\{\ln\tau_-(s)\right\}=\lim_{\varepsilon\to o}\ \frac{1}{2\pi i}\int_{-i\varepsilon}^{i\varepsilon}\frac{\ln\left\{1-\frac{B\tilde{\omega}_o}{2z}\ \ln\left(\frac{1-\tilde{\omega}_o F/2+z}{1-\tilde{\omega}_o F/2-z}\right)\right\}}{z}dz \quad (31)$$

Upon substitution of $z=\varepsilon\, e^{iW}$, we obtain

$$\lim_{s\to o}\ \left\{\ln\tau_-(s)\right\}\ =\ -\frac{1}{2}\ \ln\left\{1-\frac{B\tilde{\omega}_o}{1-\frac{\tilde{\omega}_o F}{2}}\right\} \quad (32)$$

Thus

$$\lim_{s \to o} \left\{\tau_-(s)\right\} = \left\{1 - \frac{B\tilde{\omega}_o}{1 - \frac{\tilde{\omega}_o F}{2}}\right\}^{-\frac{1}{2}}$$

$$= \sqrt{\frac{1 - \tilde{\omega}_o F/2}{1 - \tilde{\omega}_o}} \qquad (33)$$

We may now return to Equation (22), and substitute in this equation Equation (33). This results in

$$\phi_o(s) = I_o \left[\left(1 - \tilde{\omega}_o F/2\right) \Big/ \left(1 - \tilde{\omega}_o\right)\right]^{3/2} \frac{\tau_-(s)}{1 - \tilde{\omega}_o F/2 + s} \qquad (34)$$

Recall that (from Equation 7), $I(o,\mu) = -\frac{\tilde{\omega}_o B}{2\mu}\ \phi_o\left(-\frac{1 - \tilde{\omega}_o F/2}{\mu}\right)$, for all μ between -1 and 0. This making use of Equation (34) gives us

$$I(o,\mu) = \frac{\tilde{\omega}_o B}{2}\ I_o \left(1 - \tilde{\omega}_o F/2\right)^{\frac{1}{2}} \left(1 - \tilde{\omega}_o\right)^{-3/2} \frac{\tau_-\left(-\frac{1 - \tilde{\omega}_o F/2}{\mu}\right)}{1 - \mu} \qquad (35a)$$

The function $\tau_-\left(-\frac{1 - \tilde{\omega}_o F/2}{\mu}\right)$ may be evaluated from Equation (27) and results in

$$\tau_-\left(-\frac{1 - \tilde{\omega}_o F/2}{\mu}\right) = \mathrm{Exp}\left[\frac{\mu}{\pi} \int_o^{\pi/2} \frac{\ln\left\{1 - \frac{B\tilde{\omega}_o}{1 - \tilde{\omega}_o F/2} \cdot \frac{W}{\tan W}\right\}}{\mu^2\ \mathrm{Sin}^2 W + s^2\ \mathrm{Cos}^2 W}\ dW\right] \qquad (35b)$$

Finally, $I(o,\mu)$ is given by

$$I(o,\mu) = I_o \frac{\tilde{\omega}_o B}{2} \left(1 - \frac{\tilde{\omega}_o F}{2}\right)^{\frac{1}{2}} \left(1 - \tilde{\omega}_o\right)^{-3/2} \cdot \frac{1}{1-\mu} \cdot$$

$$\text{Exp}\left[\frac{\mu}{\pi} \int_o^{\pi/2} \frac{\ln\left\{1 - \frac{B\tilde{\omega}_o W \text{ Cot } W}{1 - \tilde{\omega}_o F/2}\right\}}{\mu^2 \text{ Sin}^2 W + s^2 \text{ Cos}^2 W} dW\right] \qquad (36)$$

for all μ between -1 and 0. The $I(o,\mu)$ represents the backscattered radiance received by the overhead detector in a remote sensing application. The integral involved in Equation (36) may easily be evaluated for a specific scattering angle.

Upon examination of Equation (36), it is evident that for a given scattering angle μ, the backscattered radiance depends on the scattering phase function ($P(\mu) = f(B,F)$), and the single scattering albedo $\tilde{\omega}_o$. The functional relationship between $I(o,\mu)$ and $\tilde{\omega}_o$ in our result (Equation 36) is different than the functional dependence of $I(o,\mu)$ on $\tilde{\omega}_o$ in the results obtained from quasi-single scattering approximation [5]. The difference in the two results becomes large as $\tilde{\omega}_o$ takes the values close to 1. The numerical results obtained from Equation (36) and their differences from quasi-single scattering approximation are reported in Section 4.

3.0 SCATTERING PHASE FUNCTIONS

In this section we have summarized (1) the available information on the measurements of the scattering phase functions, and (2) the calculated scattering phase functions utilizing the Mie formalism for polydispersed suspensions on the basis of size distribution measurements provided to us through the LaRC laboratory program. The compilation of this information is primarily done to determine the constants B, and F for the phase function $P(\mu)$. These constants are required to evaluate Equation (36) in Section 2.

3.1 Measured Scattering Probability Functions

Several in-site, as well as in vitro measured scattering phase functions covering turbid to clear water conditions have earlier been reported in Reference [2]. Reference [2] presents (1) observations made in lake water [12], coastal waters [13], Atlantic surface water [14], Pacific near coastal water [15], Mediterranean [16], and Sargasso Sea water [17], (2) measurements taken by the Scripps Institution of Oceanography [18] in deep clear oceanic water (Tongue of the Ocean), near shore ocean water (off shore of Southern California), and very turbid harbor water (San Diego Harbor,) (3) the observation taken in vitro by Petzold [18] to determine the effect of adding scattering and absorbing materials in the water.

From these observations, a set of scattering probability function $P_F(\theta)$, have been obtained, and are shown collectively in Figure 3-1.

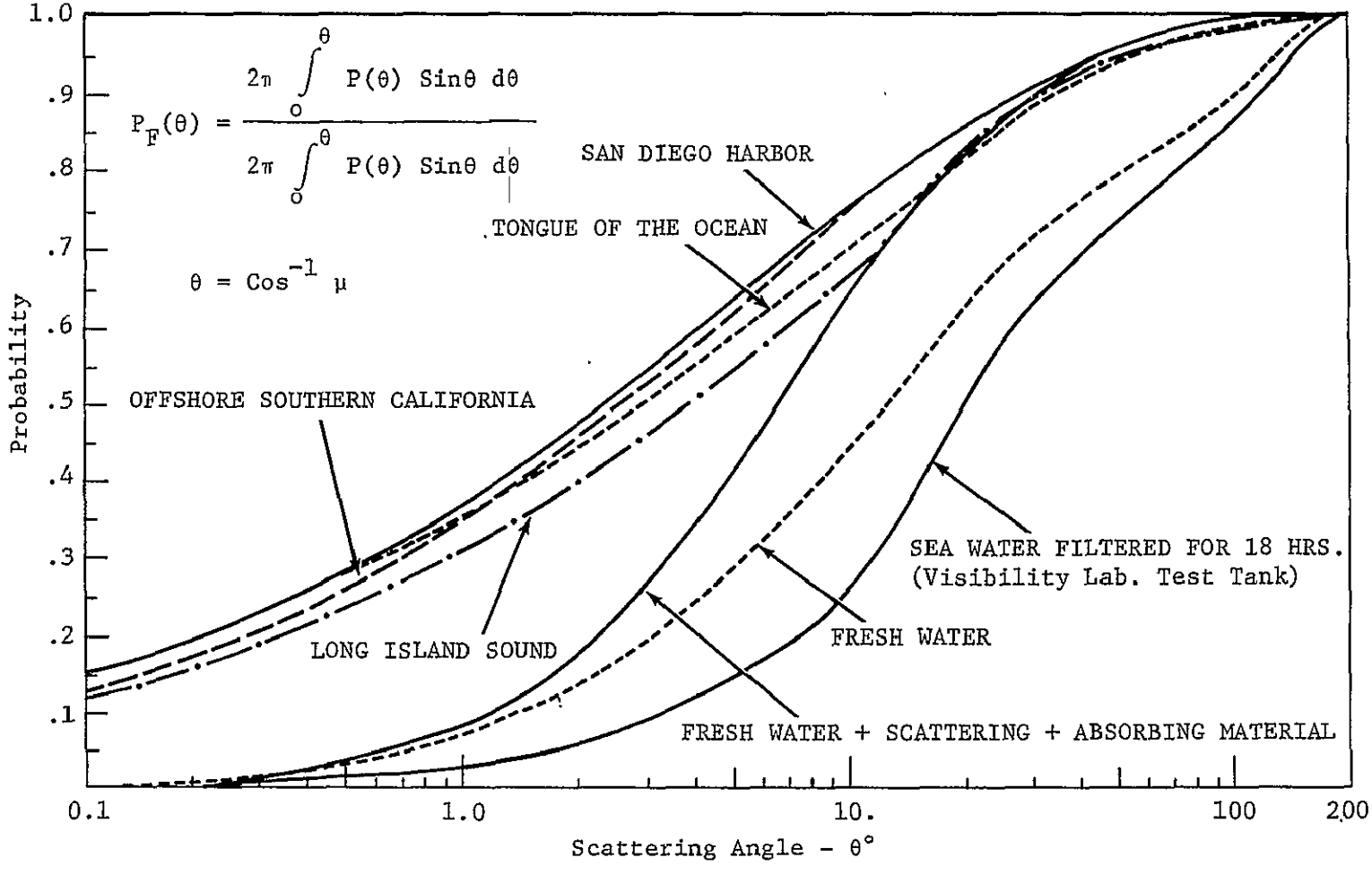

FIGURE 3.1
SCATTERING PROBABILITY FUNCTIONS FOR NATURAL OCEAN WATERS AND FOR FRESH WATER THAT HAS BEEN FILTERED AND ARTIFICIALLY MODIFIED

3.2 Calculated Scattering Probability Functions

The extension of Mie theory to the case of polydispersed suspensions has been thoroughly discussed in Reference [2] along with the computational methods used to calculate the scattering phase functions. Empirical cumulative size distribution for the 2 samples, Ball Clay, and Feldspar were provided by NASA/LaRC. These two distributions differed radically from each other, and thus allowed a reasonable investigation of the effect of different size distributions on the scattering phase functions. For both the distributions, the index of refraction (M) was chosen to have real as well as imaginary part. In order to determine the effect of absorption, the imaginary part of the index of refraction was set to zero.

The scattering probability functions obtained from Mie theory calculations utilizing these two distributions are presented in Figures 3-2 to 3-5. Two cut off limits, 100 μm and 10 μm were considered to be appropriate for the computations. The different cut off limits allow to investigate the effect of sediment settling in the water.

3.3 The Constants, B and F

From the definition of the scattering probability function, $P_F(\theta)$, the scattering phase function $P(\mu)$ is given by [see Section 1.1]:

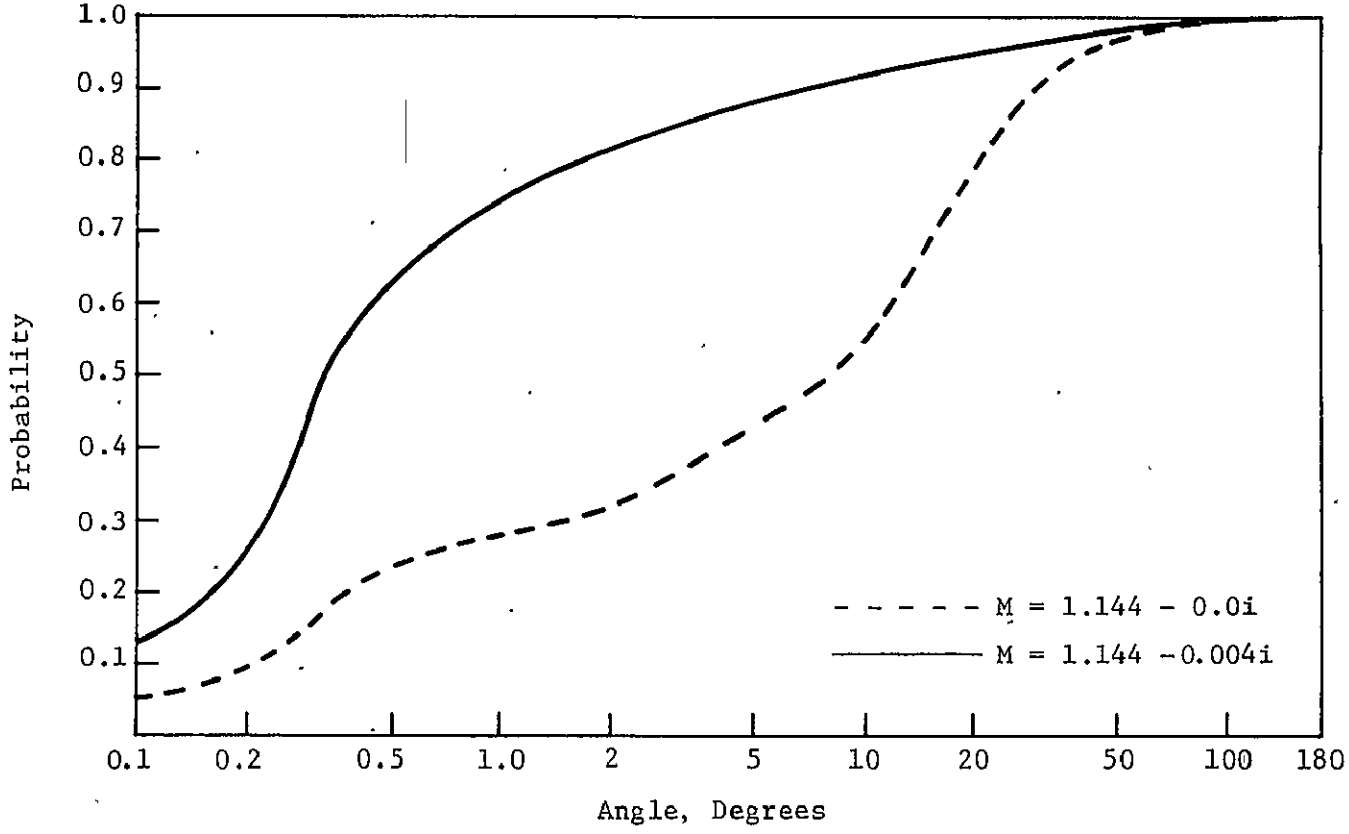

FIGURE 3.2
VOLUME SCATTERING DISTRIBUTION FUNCTIONS FOR FELDSPAR
(100μM CUT OFF λ = 500NM)

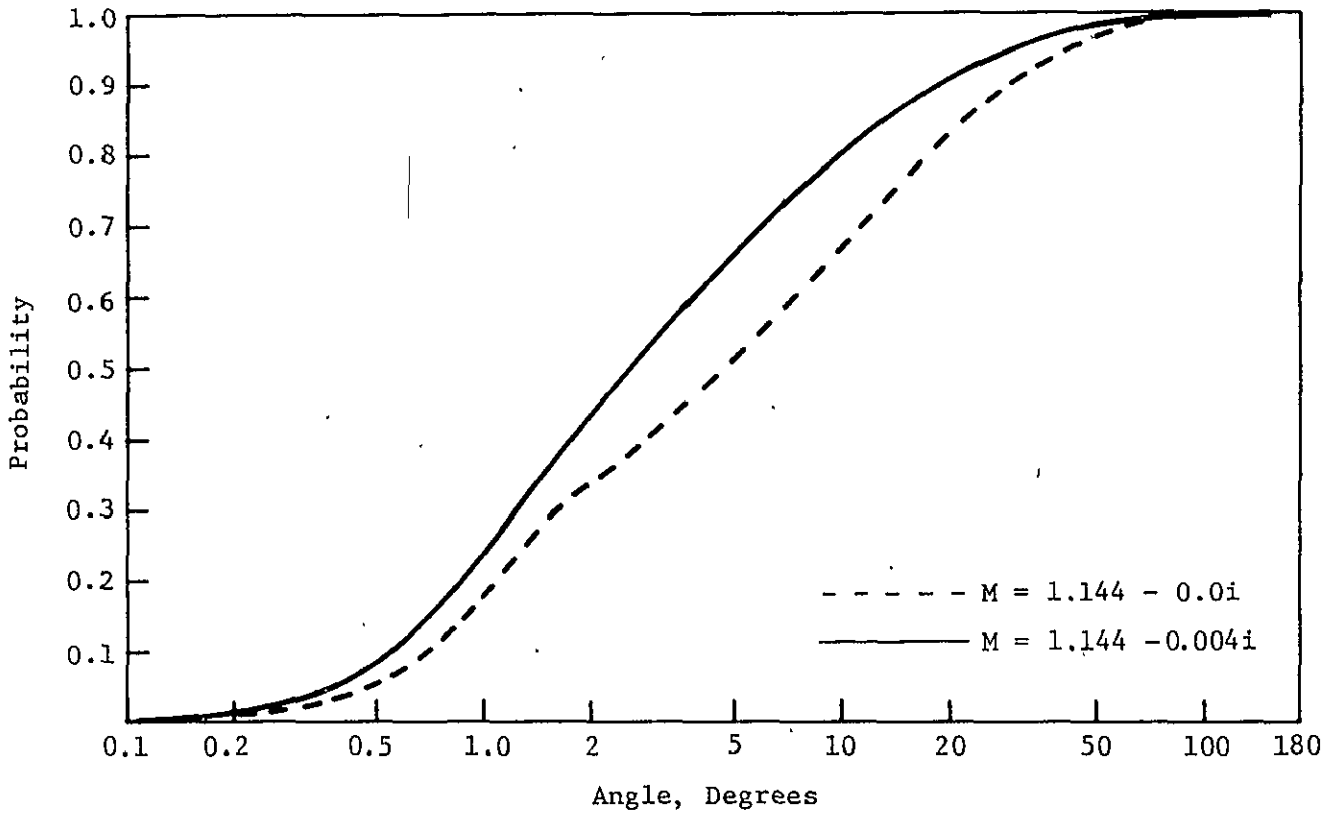

FIGURE 3.3
VOLUME SCATTERING DISTRIBUTION FUNCTIONS FOR FELDSPAR
(10μM CUT OFF λ = 500NM)

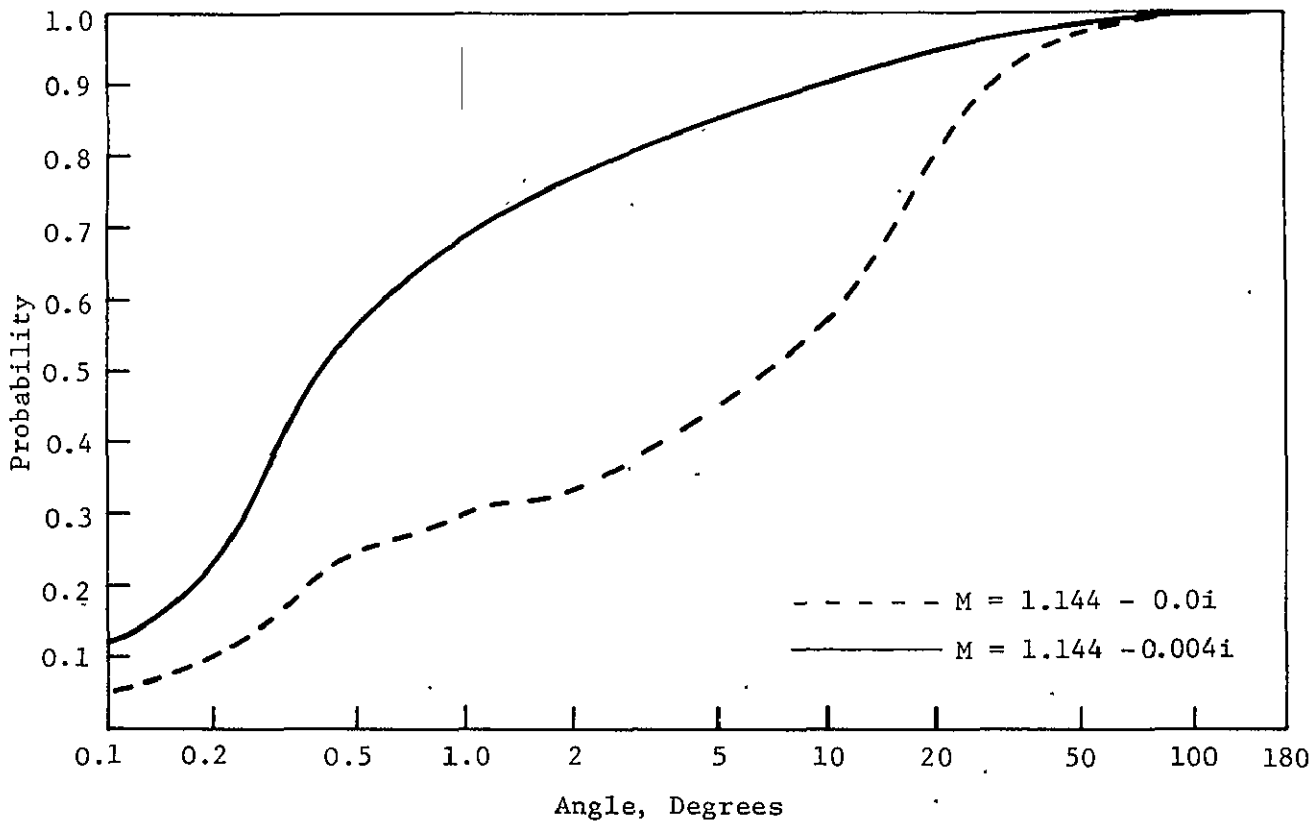

FIGURE 3.4
VOLUME SCATTERING DISTRIBUTION FUNCTIONS FOR BALL CLAY
(100μM CUT OFF λ = 500NM)

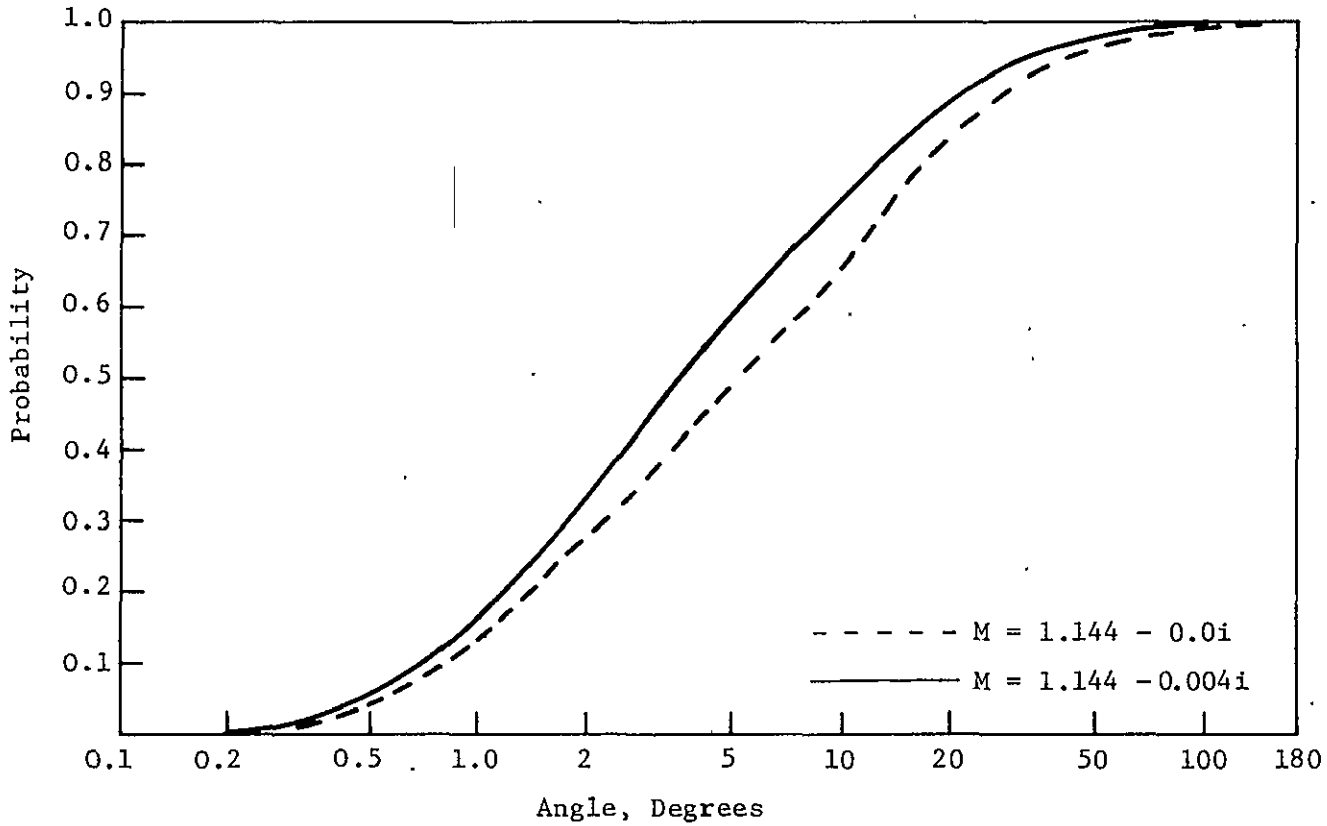

FIGURE 3.5
VOLUME SCATTERING DISTRIBUTION FUNCTIONS FOR BALL CLAY
(10μM CUT OFF λ = 500NM)

$$P_F(\Theta) = \frac{\int_{\mu}^{1} P(\mu)\, d\mu}{\int_{-1}^{1} P(\mu)\, d\mu}, \quad \mu = \cos^{-1}\Theta, \text{ and } -1 \leq \mu \leq 1.$$

Substitution of $P(\mu) = F\delta(\mu-1) + B$ (see Equation 4) results in

$$P_F(\Theta) = \frac{\int_{\mu}^{1} \left[F\delta(\mu-1) + B\right]\, du}{F + 2B} = \frac{F+B - B\mu}{F + 2B} . \qquad (37)$$

The condition, $\frac{1}{2} \int_{-1}^{1} \left[F\delta(\mu-1) + B\right] d\mu = 1$ implies

$$F + 2B = 2$$

and

$$B = \frac{2-2P_F(\Theta)}{1 + \mu} . \qquad (38)$$

The numerical values of B as determined from $P_F(\theta)$ illustrated in Figures 3-1 to 3-5 are presented in Tables 3-I and 3-II. Four water qualities, San Diego Harbor, Tongue of the Ocean, offshore Southern California, and fresh water + scattering + absorbing material were chosen to calculate the range of the values for B in Table 3-I. San Diego Harbor water represents the most turbid water of all, and gives an upper bound on the value of $B(\approx 0.06)$ for the measured scattering probability functions. The upper bound on B as determined from the calculated scattering probability functions utilizing Mie theory formulation is 0.041.

TABLE 3-I

B THE FRACTION BACKSCATTERED DETERMINED FROM IN SITU AND IN VITRO EXPERIMENTS

		WATER QUALITY			
Angle of Incidence θ	$\mu = \cos\theta$	San Diego Harbor	Tongue of The Ocean	Offshore Southern California	Fresh Water + scattering + absorbing material
45^{o}	0.707	0.0585	0.0585	0.0585	0.0468
60^{o}	0.5	0.05333	0.05333	0.05333	0.0266
70^{o}	0.324	0.0447	0.0447	0.0447	0.0223
80^{o}	0.173648	0.0341	0.0341	0.0341	0.0170
90^{o}	0.0	0.03	0.03	0.03	0.010

TABLE 3-II

B THE FRACTION BACKSCATTERED CALCULATED FROM MIE THEORY

		Sediments			
		Feldspar		Ball Clay	
Angle of Incidence θ	Cos θ	100 μ cut off	10 μ cut off	100 μ cut off	10 μ cut off
45°	0.707	.041	.039	.041	.039
60°	0.50	.038	.037	.038	.037
70°	0.342	.03	.028	.031	.029
80°	0.173648	.02	.017	.021	.018
90°	0.0	.008	.007	.008	.007

4.0 RESULTS

In this section we describe our numerical results on the back-scattered radiance determined from the solution of the radiative transport equation. Before this is done, however, we present the closed form analytical solution derived earlier and describe some of the parameters involved. The normalized backscattered radiance may be written as (see Equation 36):

$$\frac{I(o,\mu)}{I_o} = \frac{\tilde{\omega}_o B}{2}\left(1 - \frac{\tilde{\omega}_o F}{2}\right)^{1/2}\left(1 - \tilde{\omega}_o\right)^{-3/2}\frac{1}{1-\mu}\cdot$$

$$\text{Exp}\left[\frac{\mu}{\pi}\int_o^{\pi/2}\frac{\ln\left\{1 - \dfrac{B\tilde{\omega}_o W \text{ Cot } W}{1 - \tilde{\omega}_o F/2}\right\}}{\mu^2 \text{ Sin}^2 W + s^2 \text{ Cos}^2 W}\, dW\right]$$

Where I_o = Incident radiance

$\tilde{\omega}_o$ = Single scattering albedo = $\frac{s}{\alpha} = \frac{s}{s+a}$

S = Total scattering coefficient

α = Total attenuation coefficient

a = Total absorbing coefficient

μ = $\text{Cos}\theta$, θ is the scattering angle

B, and F are the parameters used to represent the phase function $P(\mu) = F\delta(\mu-1) + B$

The range of the values of B have been determined from the measured as well as calculated phase functions and is found to vary between 0.007 and 0.06. F is computed from B by a

relationship F = 2-2B, determined in Section 2.

The integration involved in Equation (39) was performed utilizing a computer code given in Appendix A. The computer program makes use of a Lobatto [19] integration algorithim.

To investigate the effect of wavelength, the single scattering albedo, $\tilde{\omega}_o$ was varied between 0.6 and 0.95. These limits on $\tilde{\omega}_o$ were arrived at from the limits on the a/s ratio which is a function of the wavelength. The a/s ratio for sediments varies between 0.20 at λ = 550 nm and 0.50 at λ = 370 nm [4]. Typical values of a/s ratio at 550 nm are between 0.06 (for quartz particles) and 0.20 for environmental waters.

The results of the calculations for backscattered radiance per unit incident radiance are presented in Figures 4-1A to 4-1G, and indicate that the backscattered radiance received by an overhead detector is very sensitive to the changes in (1) the scattering phase function $P(\mu)$ ($P(\mu) = f(B,F)$), and (2) the single scattering albedo, $\tilde{\omega}_o$.

Another observation which can be made from Figure 4-1A to 4-1G is that $\frac{\partial I(o,\mu)}{\partial \tilde{\omega}_o} >> \frac{\partial I(o,\mu)}{\partial \mu}$, i.e., for a given scattering phase function, the incremental change in the backscattered radiance w.r.t. $\tilde{\omega}_o$ is much larger than the incremental change in the backscattered radiance w.r.t. the scattering angle, μ. At the same time the function $\frac{\partial I(o,\mu)}{\partial \mu}$ varies slowly for smaller values of $\tilde{\omega}_o$ (up to $\tilde{\omega}_o$ = 0.80), and

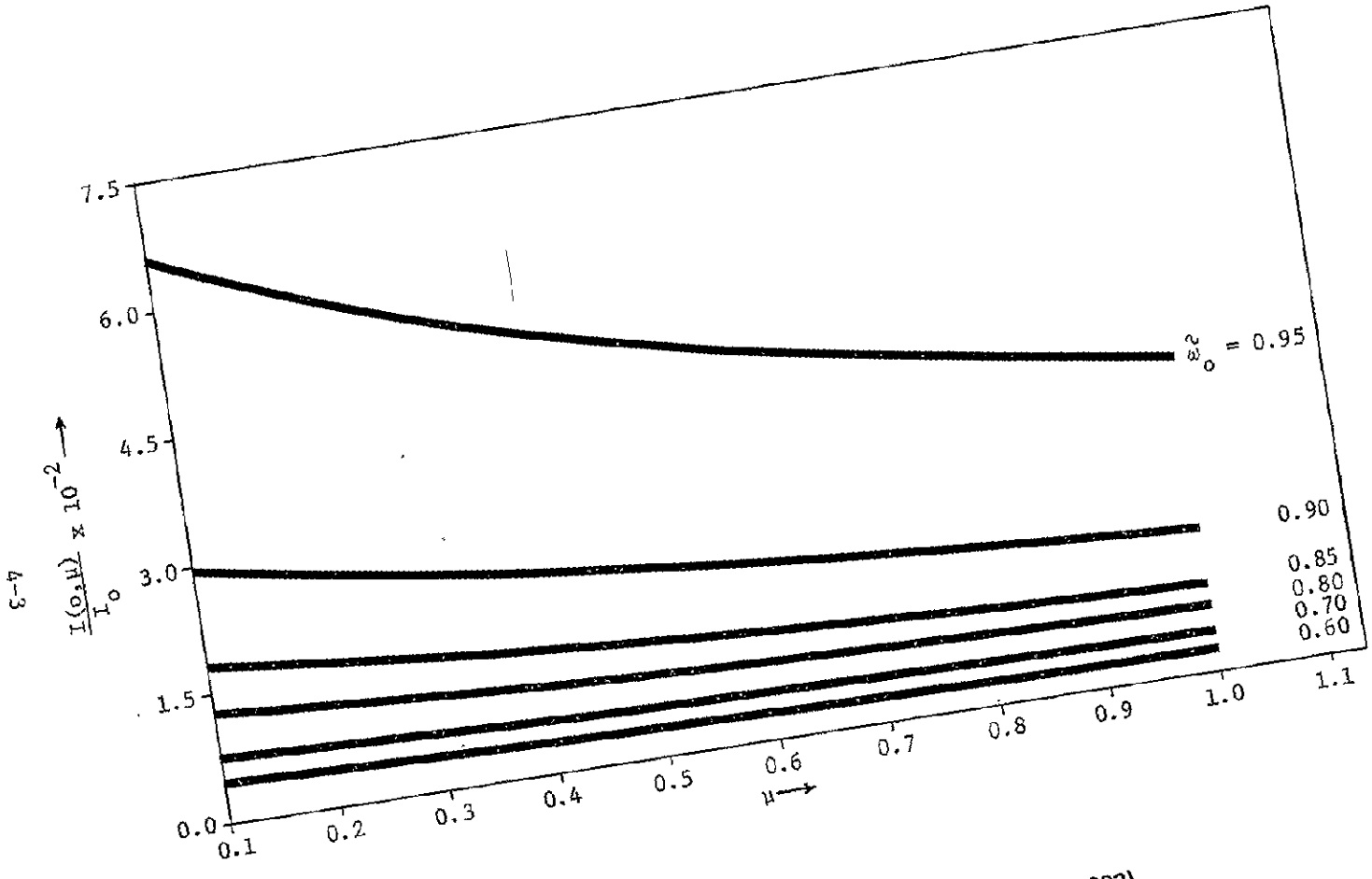

FIGURE 4.1A
RELATIVE BACKSCATTERED RADIANCE (B = 0.007, F/2 = 0.993)

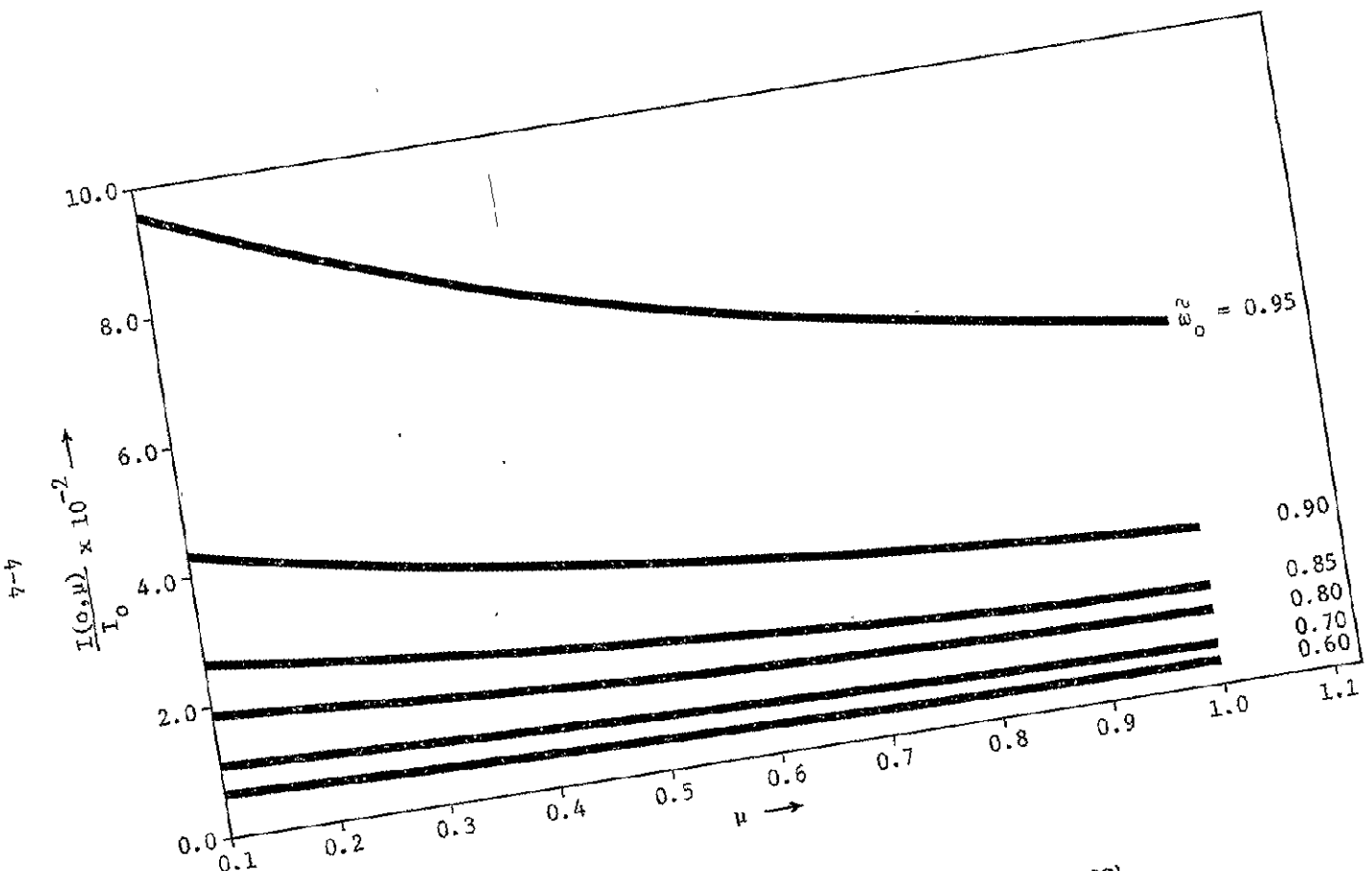

FIGURE 4.1B
RELATIVE BACKSCATTERED RADIANCE (B = 0.01, F/2 = 0.99)

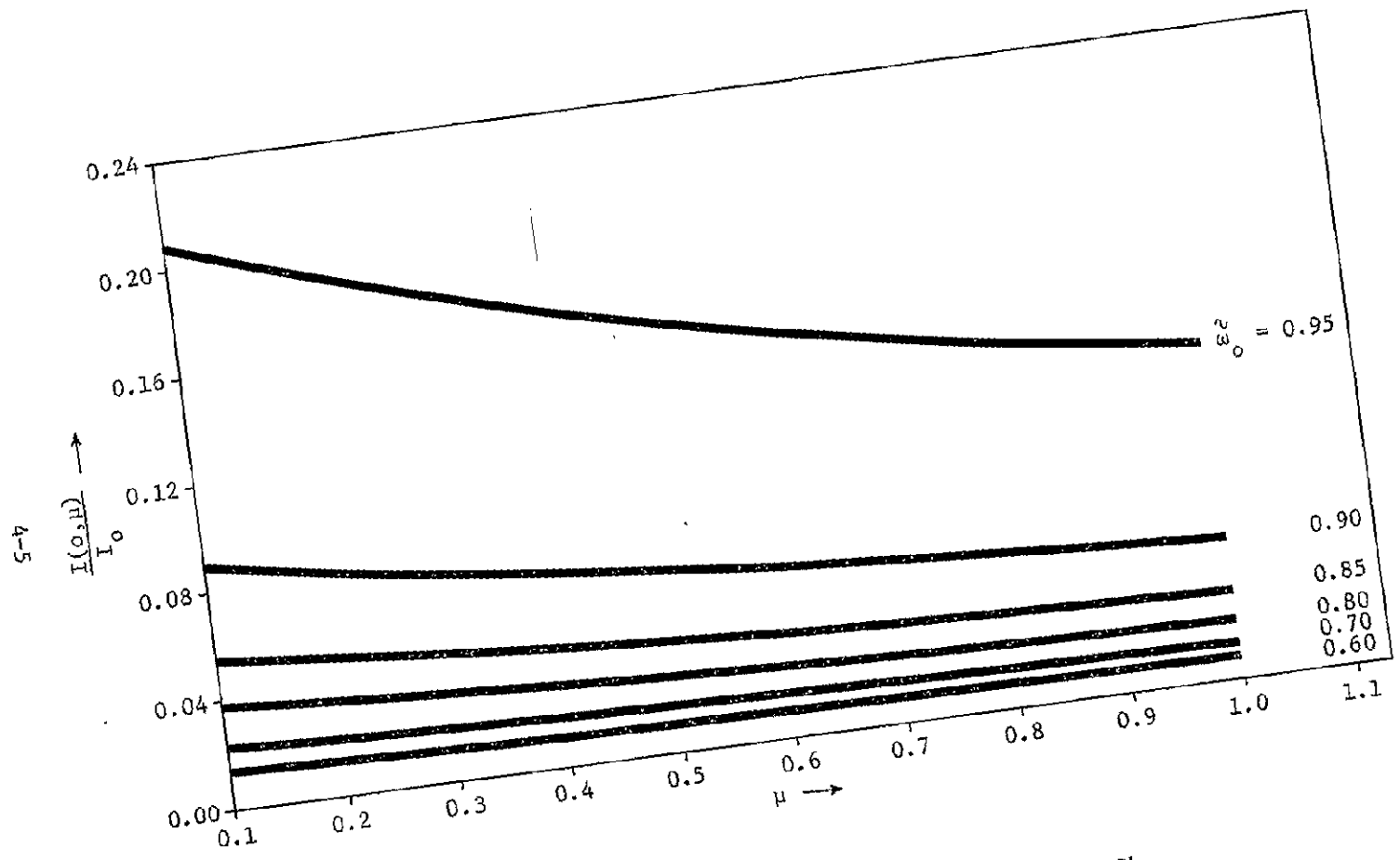

FIGURE 4.1C
RELATIVE BACKSCATTERED RADIANCE (B = 0.02, F/2 = 0.98)

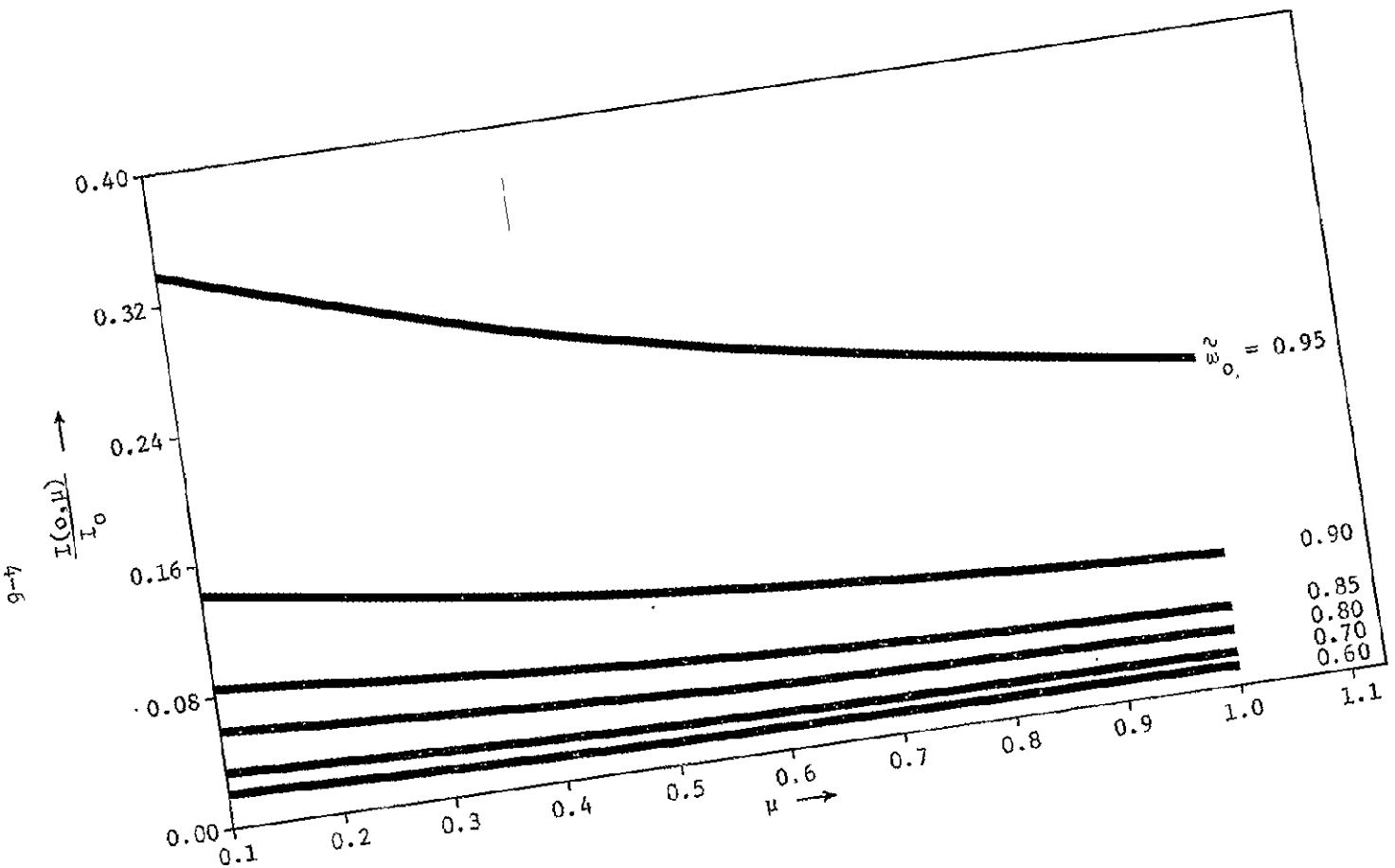

FIGURE 4.1D
RELATIVE BACKSCATTERED RADIANCE (B = 0.03, F/2 = 0.97)

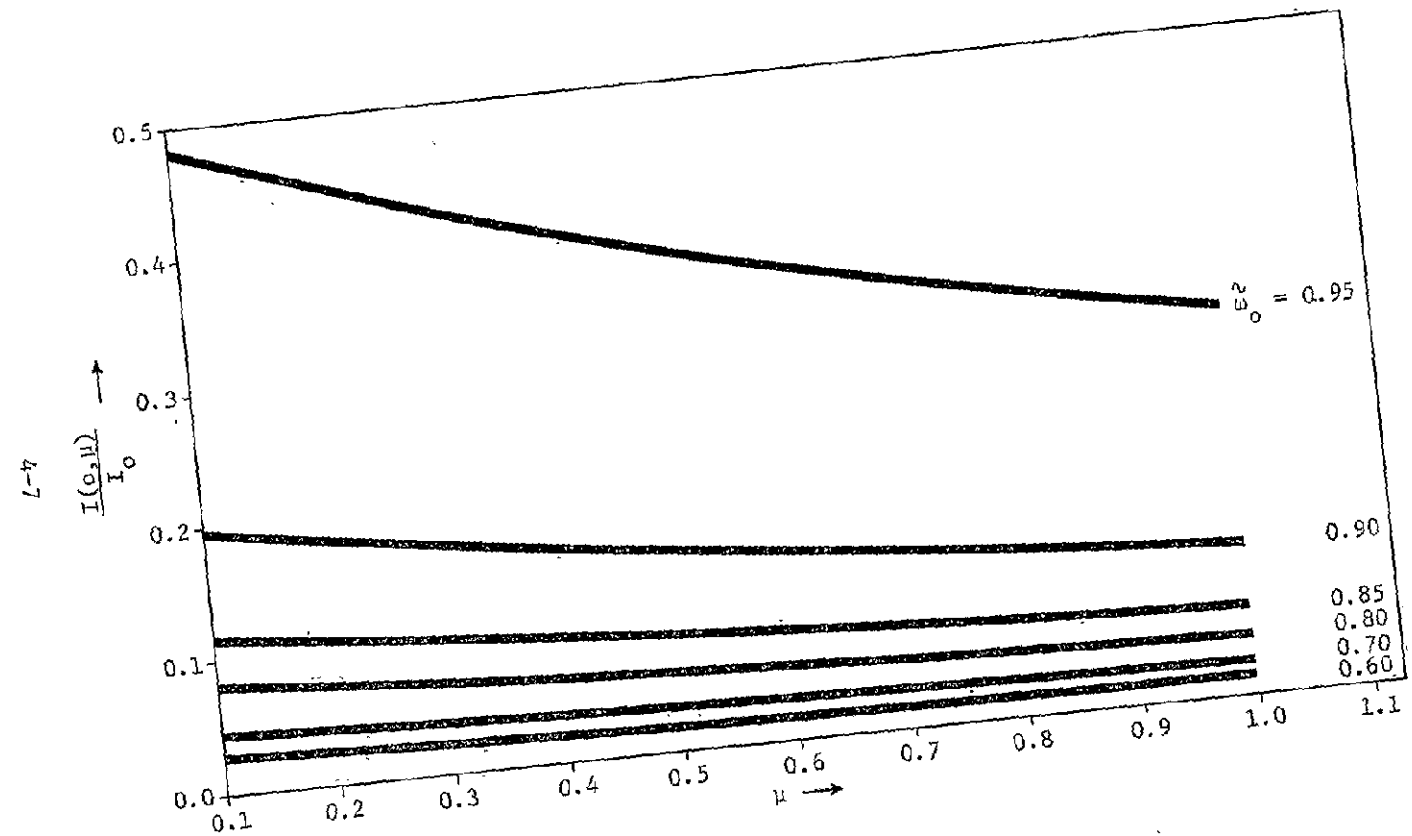

FIGURE 4.1E
RELATIVE BACKSCATTERED RADIANCE (B = 0.04, F/2=0.96)

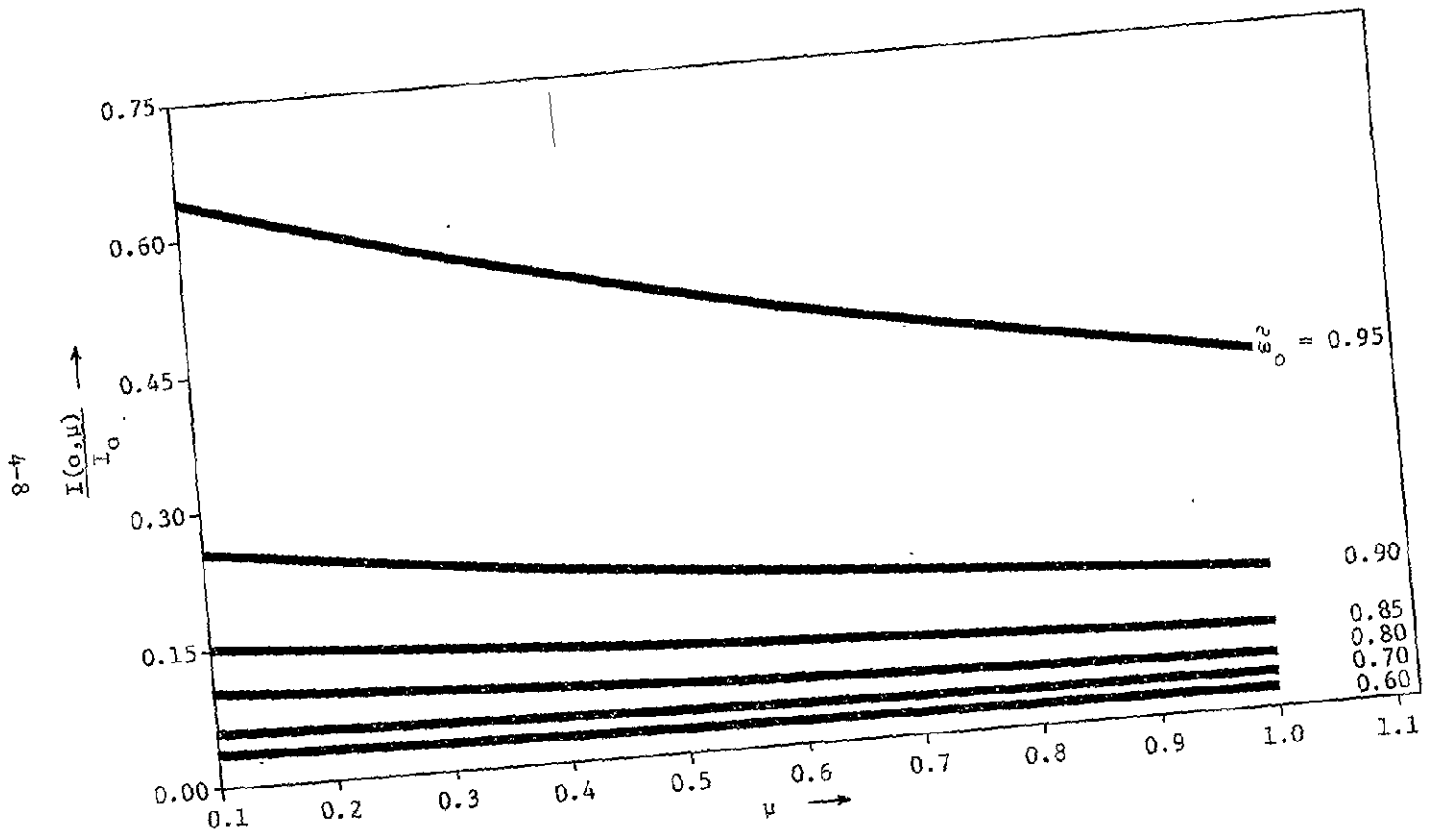

FIGURE 4.1F
RELATIVE BACKSCATTERED RADIANCE (B = 0.05, F.2 = 0.95)

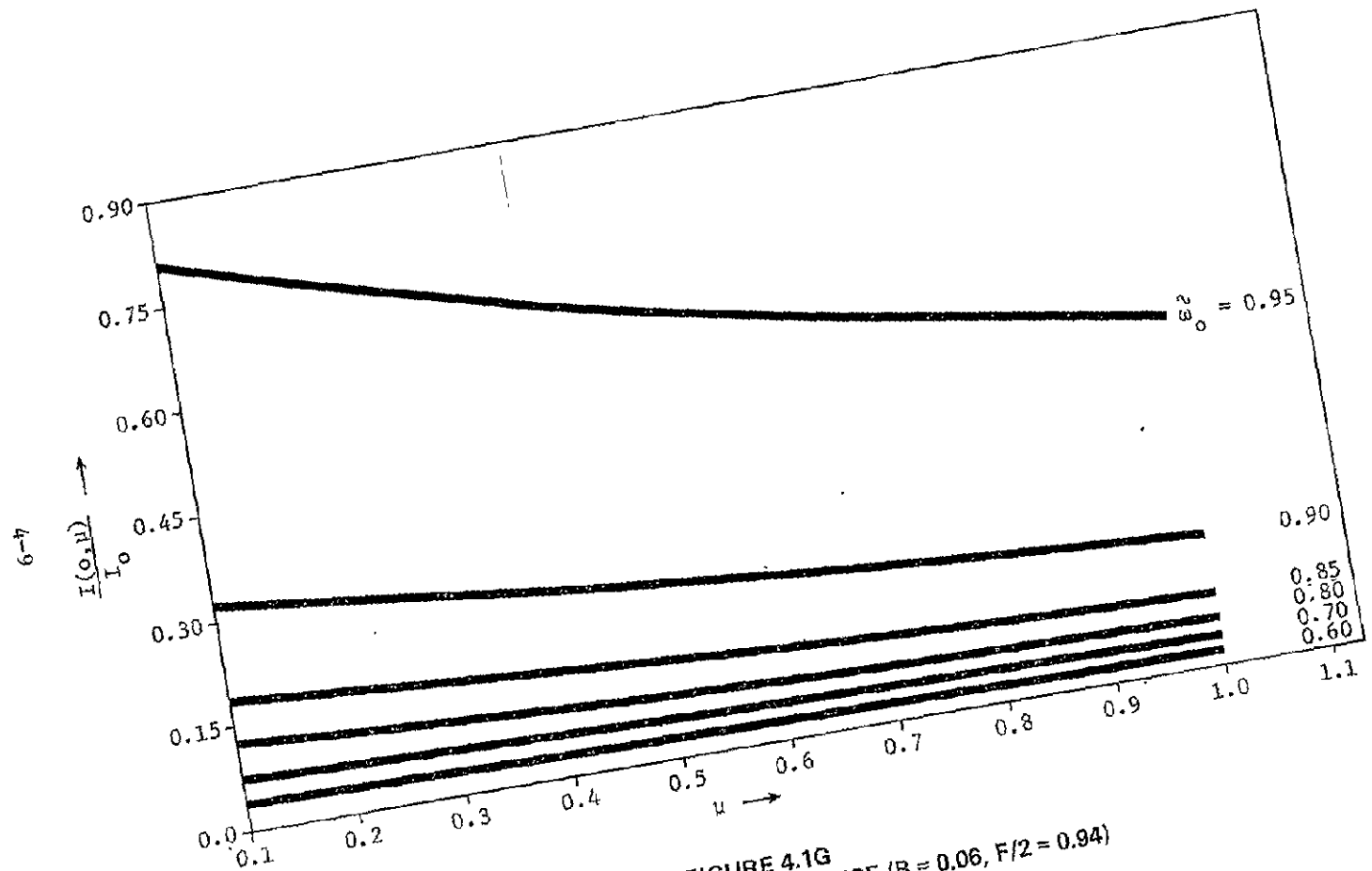

FIGURE 4.1G
RELATIVE BACKSCATTERED RADIANCE (B = 0.06, F/2 = 0.94)

attains a large value for $\tilde{\omega}_o$ close to unity. For example, for $\tilde{\omega}_o = 0.95$, and $P(\mu) = 1.88\ \delta(\mu-1) + 0.060$, the received backscattered radiance is as large as 80% of the incident radiance.

4.1 Comparison of Metrek's Results with Quasi-Single Scattering Approximation

The quasi-single scattering approximation results were earlier reported by Gordon [5]. The backscattered radiance from his results is given by (see Equation 11)

$$I_Q(o,\mu) = \frac{\tilde{\omega}_o\, P(-|\mu|)}{2\left(1 - \frac{\tilde{\omega}_o F}{2}\right)} \cdot \frac{I_o}{(1 + |\mu|)}$$

As described in Section 2.4, the above equation is equivalent to

$$I_Q(o,\mu) = \frac{\tilde{\omega}_o B}{2\left(1 - \frac{\tilde{\omega}_o F}{2}\right)} \cdot \frac{I_o}{1 - \mu} \qquad -1<\mu<o \qquad (40)$$

In that case, from equations (39) and (40), we obtain

$$I(o,\mu) = \text{FACTOR} \cdot I_Q(o,\mu) \qquad (41)$$

where

$$\text{FACTOR} = \frac{\left(1 - \frac{\tilde{\omega}_o F}{2}\right)^{3/2}}{\left(1 - \tilde{\omega}_o\right)^{3/2}} \text{EXP}\left[\frac{\mu}{\pi} \int_o^{\pi/2} \frac{\ln\left\{1 - \frac{B\tilde{\omega}_o\, W \cot W}{1 - \tilde{\omega}_o F/2}\right\}}{\mu^2 \sin^2 W + s^2 \cos^2 W}\, dW\right] \qquad (42)$$

The FACTOR was evaluated for $\tilde{\omega}_o$ ranging from 0.60 to 0.95, and B ranging from 0.007 to 0.06. The results are presented in Tables 4-I to 4-VII.

TABLE 4-I

FACTOR FOR B = 0.007 AND F/2 = 0.993

μ \ ω_o^2	0.60	0.65	0.70	0.75	0.80	0.85	0.90	0.95
0.1	1.017	1.021	1.027	1.034	1.046	1.065	1.104	1.224
0.2	1.018	1.022	1.028	1.035	1.047	1.067	1.108	1.233
0.3	1.018	1.022	1.028	1.036	1.049	1.069	1.111	1.239
0.4	1.018	1.023	1.029	1.037	1.049	1.070	1.113	1.244
0.5	1.019	1.023	1.029	1.038	1.050	1.071	1.114	1.247
0.6	1.019	1.023	1.029	1.038	1.051	1.072	1.116	1.250
0.7	1.019	1.024	1.030	1.038	1.051	1.073	1.117	1.253
0.8	1.019	1.024	1.030	1.039	1.052	1.073	1.118	1.255
0.9	1.019	1.024	1.030	1.039	1.052	1.074	1.119	1.257
1.0	1.019	1.024	1.030	1.039	1.052	1.074	1.119	1.259

TABLE 4-II

FACTOR FOR B = 0.010 AND F/2 = 0.990

μ \ ω_o	0.60	0.65	0.70	0.75	0.80	0.85	0.90	0.95
0.1	1.024	1.030	1.038	1.049	1.066	1.093	1.150	1.324
0.2	1.025	1.031	1.039	1.051	1.068	1.097	1.155	1.338
0.3	1.026	1.032	1.040	1.052	1.070	1.099	1.159	1.347
0.4	1.026	1.033	1.041	1.053	1.071	1.101	1.162	1.354
0.5	1.027	1.033	1.042	1.054	1.072	1.103	1.165	1.360
0.6	1.027	1.034	1.042	1.054	1.073	1.104	1.167	1.365
0.7	1.027	1.034	1.043	1.055	1.074	1.105	1.169	1.369
0.8	1.028	1.034	1.043	1.055	1.074	1.106	1.170	1.372
0.9	1.028	1.034	1.043	1.056	1.075	1.106	1.171	1.375
1.0	1.028	1.035	1.043	1.056	1.075	1.107	1.172	1.377

TABLE 4-III

FACTOR FOR B = 0.020 AND F/2 = 0.980

H \ 2θ°	0.60	0.65	0.70	0.75	0.80	0.85	0.90	0.95
0.1	1.049	1.061	1.077	1.099	1.133	1.190	1.306	1.680
0.2	1.051	1.063	1.080	1.103	1.138	1.197	1.319	1.711
0.3	1.052	1.065	1.082	1.105	1.141	1.202	1.328	1.733
0.4	1.053	1.066	1.083	1.107	1.144	1.206	1.335	1.750
0.5	1.054	1.067	1.084	1.109	1.146	1.209	1.340	1.764
0.6	1.054	1.068	1.085	1.110	1.148	1.212	1.344	1.775
0.7	1.055	1.068	1.086	1.111	1.149	1.214	1.348	1.785
0.8	1.055	1.069	1.087	1.112	1.151	1.216	1.351	1.793
0.9	1.056	1.069	1.087	1.113	1.152	1.217	1.354	1.800
1.0	1.056	1.070	1.088	1.113	1.152	1.219	1.356	1.806

TABLE 4-IV

FACTOR FOR B = 0.030 AND F/2 = 0.970

μ \ 2θ°	0.60	0.65	0.70	0.75	0.80	0.85	0.90	0.95
0.1	1.074	1.092	1.116	1.150	1.201	1.289	1.470	2.065
0.2	1.077	1.095	1.120	1.155	1.209	1.300	1.491	2.117
0.3	1.079	1.098	1.123	1.159	1.215	1.309	1.505	2.156
0.4	1.080	1.099	1.126	1.162	1.219	1.315	1.516	2.185
0.5	1.081	1.101	1.127	1.165	1.222	1.320	1.525	2.209
0.6	1.082	1.102	1.129	1.167	1.225	1.324	1.532	2.229
0.7	1.083	1.103	1.130	1.169	1.227	1.328	1.538	2.246
0.8	1.084	1.104	1.131	1.170	1.229	1.331	1.543	2.261
0.9	1.084	1.105	1.132	1.171	1.231	1.333	1.548	2.273
1.0	1.085	1.105	1.133	1.172	1.232	1.335	1.552	2.285

TABLE 4-V

FACTOR FOR B = 0.040 AND F/2 = 0.960

μ \ σ_{θ^2}	0.60	0.65	0.70	0.75	0.80	0.85	0.90	0.95
0.1	1.099	1.123	1.155	1.201	1.271	1.391	1.641	2.476
0.2	1.103	1.128	1.161	1.209	1.282	1.407	1.670	2.555
0.3	1.105	1.131	1.166	1.215	1.290	1.419	1.691	2.612
0.4	1.107	1.133	1.169	1.219	1.296	1.428	1.707	2.657
0.5	1.109	1.135	1.171	1.222	1.300	1.435	1.720	2.694
0.6	1.110	1.137	1.173	1.225	1.304	1.441	1.730	2.725
0.7	1.111	1.138	1.175	1.227	1.307	1.445	1.739	2.751
0.8	1.112	1.139	1.176	1.229	1.310	1.450	1.747	2.773
0.9	1.113	1.140	1.178	1.231	1.312	1.453	1.753	2.793
1.0	1.113	1.141	1.179	1.232	1.314	1.456	1.759	2.810

TABLE 4-VI

FACTOR FOR B = 0.050 AND F/2 = 0.950

ε_0^2 / F	0.60	0.65	0.70	0.75	0.80	0.85	0.90	0.95
0.1	1.124	1.154	1.195	1.253	1.342	1.495	1.818	2.914
0.2	1.129	1.160	1.203	1.264	1.357	1.517	1.857	3.022
0.3	1.132	1.165	1.208	1.271	1.367	1.532	1.885	3.101
0.4	1.135	1.168	1.213	1.276	1.374	1.544	1.906	3.164
0.5	1.137	1.170	1.216	1.281	1.380	1.553	1.923	3.216
0.6	1.138	1.172	1.218	1.284	1.385	1.561	1.938	3.259
0.7	1.140	1.174	1.221	1.287	1.389	1.567	1.950	3.296
0.8	1.141	1.176	1.222	1.290	1.393	1.573	1.960	3.328
0.9	1.142	1.177	1.224	1.292	1.396	1.578	1.969	3.357
1.0	1.143	1.178	1.226	1.294	1.399	1.582	1.977	3.381

TABLE 4-VII

FACTOR FOR B = 0.060 AND F/2 = 0.940

μ \ ε_0^2	0.60	0.65	0.70	0.75	0.80	0.85	0.90	0.95
0.1	1.150	1.186	1.236	1.306	1.415	1.603	2.002	3.376
0.2	1.155	1.194	1.245	1.319	1.433	1.630	2.051	3.517
0.3	1.159	1.199	1.252	1.328	1.445	1.649	2.087	3.622
0.4	1.162	1.203	1.257	1.335	1.455	1.664	2.114	3.705
0.5	1.165	1.206	1.261	1.340	1.462	1.675	2.136	3.774
0.6	1.167	1.208	1.264	1.344	1.468	1.685	2.155	3.832
0.7	1.169	1.210	1.267	1.348	1.474	1.693	2.171	3.882
0.8	1.170	1.212	1.269	1.351	1.478	1.701	2.184	3.925
0.9	1.171	1.214	1.271	1.354	1.482	1.707	2.196	3.963
1.0	1.172	1.215	1.273	1.356	1.485	1.712	2.206	3.997

It is apparant that for smaller values of B(=0.02), as well as $\tilde{\omega}_o$ (=0.80), the difference in the METREK and Gordon's results is of the order of 15 percent. At higher values of $\tilde{\omega}_o$ (=0.95), and B(=0.06), the difference in the two results becomes significant and is of the order of many magnitudes.

It must be noted that the value $\tilde{\omega}_o = 0.95$ signifies almost a totally scattering medium and in the absence of no absorption, one may expect to receive back all the radiance incident on the surface of the water. Such situations may occur in the middle of the ocean where the waters are almost turbidity free. For the LaRC experimental facility the values of $\tilde{\omega}_o$ larger than 0.80 are not expected. The water tank bottom at the LaRC's facility absorbs some of the light photons, and $\tilde{\omega}_o$ remains mostly under 0.80, in which case the results computed for $\tilde{\omega}_o > 0.80$, and presented in this section may become meaningless.

In conclusion, in this report:

1) We have presented a mathematical formalism applicable to the radiative transport process for the geometry of the light scattering relevant to the LaRC laboratory experiment set up. Then an analytical solution to this equation has been derived to determine the backscattered radiance as a function of the single scattering albedo $\tilde{\omega}_o$, incident radiance I_o, and the scattering phase function $P(\mu)$.

2) The results measured as well as calculated scattering phase functions for a wide range of turbid water conditions are summarized to determine the lower and upper bounding scattering phase functions. The bounding scattering phase functions have been used to obtain a better estimate of the ranges of the parameters involved in the scattering phase function formulation.

3) The solution derived for the radiative transport equation is numerically evaluated for a range of scattering phase functions, and also for a range of single scattering albedo.

Finally,

4) METREK's results are compared with the already reported results in the literature on quasi-single scattering approximation.

The differences between the two results have been discussed in Section 4.1.

APPENDIX A

LOBATTO INTEGRATION COMPUTER CODE

```
C                          MAIN PROGRAM 'QUADD'
C       THIS PROGRAM PERFORMS THE DESIRED INTEGRATION AND DETERMINES
C       THE RESULTANT RADIANCE RECEIVED BY THE REMOTE SENSOR.
C
C    LOBATTO INTEGRATION
C    DESCRIPTION OF PARAMETERS
C       A-      LOWER LIMIT
C       B-      UPPER LIMIT
C       E-      PRECISION
C       FCT-    SUBROUTINE FCT(X,Y)
C                 Y=F(X)
C                 USE EXTERNAL FCT IN MAIN PROGRAM
C       N-      SET EQUAL TO 200
C       AUX-    STORAGE FOR CALCULATED VALUES OF FCT,DIMENSION TO 400
C       ICHECK-   <0, NOT CONVERGED WITH REQUIRED PRECISION
C                 >0, CONVERGED, NO. OF CYCLES REQUIRED
C       V-      ANSWER
C       ARRAY-  ARRAY OF PARAMETERS IN FCT, USE COMMON ARRAY IN FCT
C       IPARA-  NO. OF PARAMETERS IN ARRAY
C
      IMPLICIT REAL*8(A-H,O-Z)
      DIMENSION AUX(5000),BBB(7),TAU(10,8),AU(10),RAD(10,8),AAA(8)
      COMMON/XXX/ARRAY(20)
      PI=3.14159
      BBB(1)=0.007
      BBB(2)=0.01
      BBB(3)=0.02
      BBB(4)=0.03
      BBB(5)=0.04
      BBB(6)=0.05
      BBB(7)=0.06
      AAA(1)=0.60
      AAA(2)=0.65
      AAA(3)=0.70
      AAA(4)=0.75
      AAA(5)=0.80
      AAA(6)=0.85
      AAA(7)=0.90
      AAA(8)=0.95
      DO 35 J=1,7
      BB=BBB(J)
      F=2*(1.-BB)
      FF=F/2.
      WRITE(6,99)BB,FF
   99 FORMAT('1',///,15X,'B =',F6.3,5X,'F/2 =',F6.3,////)
      L=0
      DO 25 K=1,8
      L=L+1
```

```
      OMEGA=AAA(K)
      E=0.00001
      DO 25 I=1,10
      IPARA=4
      A=0.000001
      B=PI/2.
      E=0.000001
      ARRAY(1)=FLOAT(I)/10.
      ARRAY(2)=BB
      ARRAY(3)=OMEGA
      ARRAY(4)=F
      AU(I)=FLOAT(I)/10.
      EXTERNAL FCT
      N=2000
      CALL SPINT(A,B,E,FCT,N,AUX,ICHECK,V,MODE)
      AS=-ARRAY(1)*V/PI
      S1=DEXP(AS)
      S11=S1*((1.-OMEGA*F/2.)**1.5)/((1.-OMEGA)**1.5)
      S2=1/(1.+ARRAY(1))
      S3=S2/(1.-OMEGA*F/2.)
      S4=S3*OMEGA*BB/2.
      S5=S4*S11
      TAU(I,L)=S11
      RAD(I,L)=S5
      WRITE(7,115)ARRAY(1),S5
  115 FORMAT(2F8.5)
   25 CONTINUE
      DO 116 I=1,10
  116 WRITE(6,117)AU(I),(TAU(I,L),L=1,8)
  117 FORMAT(2X,F5.1,8(2X,F8.3))
      WRITE(6,119)
  119 FORMAT(////)
      DO 118 I=1,10
  118 WRITE(6,117)AU(I),(RAD(I,L),L=1,8)
   35 CONTINUE
      STOP
      END
```

```
C
C
      SUBROUTINE  SPINT(A,B,E,FCT,N,AUX,ICHECK,V,MODE)
      IMPLICIT REAL*8(A-H,O-Z)
      DIMENSION AUX(1)
    1 IF(N.LT.12) N=12
      IF(A.EQ.B) GOTO 650
      IK=(N-4)/8
      IDV=2
      IX=IK+2
      IP=2*IK+3
      IFM=4*IK+3
      IFE=6*IK+3
      VC=1.D0
      AA=A
      BB=B
      IF(A.LT.B) GOTO 10
      AA=B
      BB=A
      VC=-1.D0
   10 A0=0.0476190476190476D0
      A1=0.2768260473615659D0
      A2=0.4317453812098626D0
      A3=0.4876190476190476D0
      T5=0.8302238962785669D0
      T4=0.4688487934707142D0
      T2=-T4
      T1=-T5
C
C     FIRST INTERVAL (A TO B)
      C=0.50*(BB-AA)
      D=AA+C
      X1=C*T1+D
      X2=C*T2+D
      X4=C*T4+D
      X5=C*T5+D
      CALL FCT(AA,AUX(IFE+1))
      CALL FCT(X1,F1)
      CALL FCT(X2,F2)
      CALL FCT(D,AUX(IFM+1))
      CALL FCT(X4,F4)
      CALL FCT(X5,F5)
      CALL FCT(BB,AUX(IFE+2))
      V0=C*(A0*(AUX(IFE+1)+AUX(IFE+2))+A1*(F1+F5)+A2*(F2+F4)+A3*AUX(IFM+
     11))
C
C     SPLIT FIRST INTERVAL
      K=1
```

```
      C=0.5D0*C
      V=0.D0
      AUX(IFE+3)=AUX(IFE+2)
      AUX(IFE+2)=AUX(IFM+1)
      DO 100 I=1,2
      D=AA+FLOAT(I+I-1)*C
      X1=C*T1+D
      X2=C*T2+D
      X4=C*T4+D
      X5=C*T5+D
      CALL FCT(X1,F1)
      CALL FCT(X2,F2)
      IFMI=IFM+I
      CALL FCT(D,AUX(IFMI))
      CALL FCT(X4,F4)
      CALL FCT(X5,F5)
      IFEI=IFE+I
      IPI=IP+I
      AUX(IPI)=C*(A0*(AUX(IFEI)+AUX(IFEI+1))+A1*(F1+F5)+A2*(F2+F4)+A3*AU
     1X(IFMI))
  100 V=V+AUX(IPI)
C
C     CHECK CONVERGENCE
      IF(V.EQ.V0) GOTO 9000
      AUX(IDV+1)=V-V0
      VA=DABS(V)
      IF(VA.EQ.0.0) VA=DABS(V0)
      IF(DABS(AUX(IDV+1))/VA.LT.E) GOTO 9000
      IF(IK.EQ.1) GOTO 500
C     END OF INITIAL CALCULATIONS
C
C     BEGIN SELECTIVE SPLITTING PROCESS
      SDS=AUX(IDV+1)
      AUX(IX+1)=AA
      AUX(IX+2)=BB
      IT=1
C
C     RESET VALUES
 1000 K=K+1
      IB=IT+1
      I1=IB+1
      IXIT=IX+IT
      C=0.125D0*(AUX(IXIT+1)-AUX(IXIT))
      V0=V
      IDVIT=IDV+IT
      SDS=SDS-AUX(IDVIT)
      IR=IT+IT-1
      IPIR=IP+IR
```

```
      V=V-AUX(IPIR)-AUX(IPIR+1)
      IXK=IX+K
      AUX(IXK+1)=AUX(IXK)
      KTW=2*K+1
      IFEKTW=IFE+KTW
      AUX(IFEKTW)=AUX(IFEKTW-2)
      IF(K.EQ.IB) GOTO 105
      DO 104 I=I1,K
      L=K+I1-I
      LXL=IX+L
      AUX(IXL)=AUX(IXL-1)
      IDVL=IDV+L
      AUX(IDVL)=AUX(IDVL-1)
      IZ=2*L-1
      IFEIZ=IFE+IZ
      AUX(IFEIZ)=AUX(IFEIZ-2)
      AUX(IFEIZ+1)=AUX(IFEIZ-1)
      IFMIZ=IFM+IZ
      AUX(IFMIZ)=AUX(IFMIZ-2)
      AUX(IFMIZ+1)=AUX(IFMIZ-1)
      IPIZ=IP+IZ
      AUX(IPIZ)=AUX(IPIZ-2)
  104 AUX(IPIZ+1)=AUX(IPIZ-1)
  105 AUX(IXIT+1)=AUX(IXIT)+4.*C
C
C     SPLIT LOOP
      IFEIR=IFE+IR
      AUX(IFEIR+2)=AUX(IFEIR+1)
      IFMIR=IFM+IR
      AUX(IFEIR+1)=AUX(IFMIR)
      AUX(IFEIR+3)=AUX(IFMIR+1)
      AUX(1)=AUX(IPIR)
      AUX(2)=AUX(IPIR+1)
      L=0
      DO 300 J=1,2
      SA=0.D0
      DO 200 I=1,2
      L=L+1
      LV=IT+IT-2+L
      D=AUX(IXIT)+FLOAT(L+L-1)*C
      X1=C*T1+D
      X2=C*T2+D
      X4=C*T4+D
      X5=C*T5+D
      CALL FCT(X1,F1)
      CALL FCT(X2,F2)
      IFMLV=IFM+LV
      CALL FCT(D,AUX(IFMLV))
```

```
      CALL FCT(X4,F4)
      CALL FCT(X5,F5)
      IFELV=IFE+LV
      AI=C*(A0*(AUX(IFELV)+AUX(IFELV+1))+A1*(F1+F5)+A2*(F2+F4)+A3*AUX(IF
     1ILV))
      SA=SA+AI
      IPLV=IP+LV
  200 AUX(IPLV)=AI
      V=V+SA
      JIT=IT+J-1
      IDVJIT=IDV+JIT
      AUX(IDVJIT)=SA-AUX(J)
  300 SDS=SDS+AUX(IDVJIT)
C
C     CHECK CONVERGENCE
      IF(V.EQ.V0) GOTO 9000
      VA=DABS(V)
      IF(VA.EQ.0.0) VA=DABS(V0)
      IF(DABS(SDS)/VA.LT.E) GOTO 9000
      IF(K.EQ.IK) GOTO 500
C
C     FIND LARGEST DELTA (WHERE TO SPLIT NEXT)
      DVMAX=DABS(AUX(IDV+1))
      DO 400 I=1,K
      IDVI=IDV+I
      ADV=DABS(AUX(IDVI))
      IF(ADV.LT.DVMAX) GOTO 400
      DVMAX=ADV
      IT=I
  400 CONTINUE
      GOTO 1000
 9000 V=V*VC
      ICHECK=K
      RETURN
  500 V=V*VC
      ICHECK=-K
      RETURN
  650 V=0.D0
      RETURN
      END
```

```
C
C
      SUBROUTINE FCT(X,Y)
      IMPLICIT REAL*8(A-H,O-Z)
      COMMON/XXX/ARRAY(20)
      Z1=ARRAY(1)*ARRAY(1)*DSIN(X)*DSIN(X)+DCOS(X)*DCOS(X)
      Z2=ARRAY(2)*ARRAY(3)/(1.-ARRAY(3)*ARRAY(4)/2.)
      Z3=X/DTAN(X)
      Z4=DLOG(1.-Z2*Z3)
      Y=Z4/Z1
      RETURN
      END
```

REFERENCES

(1) A.H. Ghovanlou, J.N. Gupta, and R.G. Henderson, "Determination of Scattering Functions and Their Effects on Remote Sensing of Turbidity in Natural Waters," The MITRE Corporation, NASA CR-145239, July 1977.

(2) A.H. Ghovanlou, J.N. Gupta, R.G. Henderson, and L. Poole, "Radiative Transfer Model For Remote Sensing of Suspended Sediments in Water," presented at the 4th Joint Conference on Sensing of Environmental Pollutants, November 6-11, New Orleans, LA.

(3) A.H. Ghovanlou, et.al., "Laser Transmission Studies of East Coast Waters, Technical Report No. 2, sponsored jointly by Office of Naval Research, Geography Branch, and The National Ocean Survey, Engineering Department Laboratory, and The U.S. Geological Survey, March 1973.

(4) A.H. Ghovanlou, "Analytical Model For Remote Sensing of Water Turbidity," The MITRE Corporation, NASA CR-145050, September 1976.

(5) H.R. Gordon, "Simple Calculation of the Diffuse Reflectance of The Ocean," Applied Optics, Vol. 12, No. 12, December 1973.

(6) V. Granatstein, M. Rhinewine, A. Levine, D. Feinstein, M. Mazurowski, and K. Piech, "Multiple Scattering of Laser Light From A Turbid Medium," Applied Optics, Vol. 11, No. 5, May 1972.

(7) K.M. Watson, J. Math, Phys., 10, 688, 1969.

(8) Y.N. Barabanekov and V. Finkelbery, Soviet Physics JETP 26, 587, 1968.

(9) G. Miltonwing, An Introduction To Transport Theory, John Wiley and Sons, Dec., New York, 1962.

(10) E. Titchmarsh, The Theory of Functions, The Clarendon Press, Oxford, 1932.

(11) R.V. Churchill, Complex Variables and Applications, McGraw Hill Book Company, New York, 1960.

(12) S.Q. Duntly, "Light in the Sea," J. Opt. Soc. America, Vol. 53, No. 2, February 1963.

REFERENCES (Concluded)

(13) G. Kullenberg, Rep Inst, Fys, Oceanog., 5, 16. Kobenhauns Universitet., 1969.

(14) N.G. Jerlov, Medd. Oceanog, Inst. Goteborg, 30, 1961.

(15) J.E. Tyler, Limm, and Oceanog., 6, 1961.

(16) G. Kullenberg and O. Berg, Rep. Inst. Fys. Oceanog., 19, 40, Kobenhavns Universitet, 1972.

(17) G. Kullenberg, Deep Sea Res., 15, 1968.

(18) T.J. Petzold, "Volume Scattering Functions for Selected Ocean Waters," AD-753474, Scripps Institution of Oceanography, October 1972.

(19) M. Abramowitz, and I. Stegum, Editors, "Handbook of Mathematical Functions," Dover Publications, Inc., New York, 1970.

DISTRIBUTION LIST

A-10

G. MacDonald

D-10

S. Blum
W. Gouse
C. Zraket

D-11

W. Sievers

D-12

H. Benington
C. Grandy
A. Tachmindji

W-50

R. Greeley
R. Ouellette
J. Golden
R. Pikul
R. Foreman
D. Sluyter

W-51

E. Sharp
L. Gsellman

W-52

M. Scholl
G. Bennington
S. Goldstein

W-53

T. Wright
E. Ward
Ali Ghovanlou (10)
W. Flury
T. Kuch
M. Barbier
O. Farah
E. Friedman
J. Gupta (10)
E. Keitz
R. Henderson
N. Lord

W-54

E. Krajeski

W-55

A. Challis**
N. Coates
J. Stone

W-56

L. Thomas
S. Lubore
G. Erskine

W-57

S. Lewis

W-50 Library (5)

Metrek Library

Technical Report Center (2)

Document Control (8)

Westpart Storage* (15)

EXTERNAL DISTRIBUTION LIST

	No. of Copies
NASA Langley Research Center Hampton, VA 23665 Attn: Report & Manuscript Control Office Mail Stop 180A	2
Lamont R. Poole, Mail Stop 272	59
NASA Ames Research Center Moffett Field, CA 94035 Attn: Library, Mail Stop 202-3	1
NASA Dryden Flight Research Center P. O. Box 273 Edwards, CA 93523 Attn: Library	1
NASA Lyndon B. Johnson Space Center 2101 Webster Seabrook Road Houston, TX 77058 Attn: JM6/Library	1
NASA Marshall Space Flight Center Marshall Space Flight Center, AL 35812 Attn: Library, AS61L	1
Jet Propulsion Laboratory 4800 Oak Grove Drive Pasadena, CA 91103 Attn: Library, Mail Stop 111-113	1
NASA Lewis Research Center 21000 Brookpark Road Cleveland, OH 44135 Attn: Library, Mail Stop 60-3	1
NASA John F. Kennedy Space Center Kennedy Space Center, FL 32899 Attn: Library, NWSI-D	1
National Aeronautics & Space Administration Washington, D.C. 20546 Attn: ER	1

EXTERNAL DISTRIBUTION LIST (Concluded)

	No. of Copies
NASA Scientific & Technical Information Facility 6571 Elkridge Landing Road Linthicum Heights, MD 21090	30